CHARACTERISTICS OF ATMOSPHERIC CIRCULATION PATTERNS ASSOCIATED WITH EXTREME TEMPERATURES OVER NORTH AMERICA IN OBSERVATIONS AND CLIMATE MODELS

By

PAUL C. LOIKITH

A dissertation submitted to the

Graduate School-New Brunswick

Rutgers, The State University of New Jersey

in partial fulfillment of the requirement

for the degree of

Doctor of Philosophy

Graduate Program in Atmospheric Science

written under the direction of

Anthony J. Broccoli

and approved by

_____

_____

_____

_____

New Brunswick, New Jersey

October, 2012

ABSTRACT OF THE DISSERTATION

Characteristics of Atmospheric Circulation Patterns Associated with Extreme Temperatures over North America in Observations and Climate Models

By

PAUL C. LOIKITH

Dissertation Director:

Anthony J. Broccoli

Motivated by a desire to understand the physical mechanisms involved in future anthropogenic changes in extreme temperature events, the key atmospheric circulation patterns associated with extreme daily temperatures over North America in the current climate are identified. Several novel metrics are used to systematically identify and describe these patterns for the entire continent. The orientation, physical characteristics, and spatial scale of these circulation patterns vary based on latitude, season, and proximity to important geographic features (i.e., mountains, coastlines). The anomaly patterns associated with extreme cold events tend to be similar to, but opposite in sign of, those associated with extreme warm events, especially within the westerlies, and tend to scale with temperature in the same locations.

The influence of the Pacific North American (PNA) pattern, the Northern Annular Mode (NAM), and the El Niño-Southern Oscillation (ENSO) on extreme temperature days and months shows that associations between extreme temperatures and the PNA and NAM

are stronger than associations with ENSO. In general, the association with extremes tends to be stronger on monthly than daily time scales. Extreme temperatures are associated with the PNA and NAM in locations typically influenced by these circulation patterns; however many extremes still occur on days when the amplitude and polarity of these patterns do not favor their occurrence. In winter, synoptic-scale, transient weather disturbances are important drivers of extreme temperature days; however these smaller-scale events are often concurrent with amplified PNA or NAM patterns. Associations are weaker in summer when other physical mechanisms affecting the surface energy balance, such as anomalous soil moisture content, are associated with extreme temperatures.

Analysis of historical runs from seventeen climate models from the CMIP5 database suggests that most models simulate realistic circulation patterns associated with extreme temperature days in most places. Model-simulated patterns tend to resemble observed patterns better in the winter than the summer and at 500 hPa than at the surface. There is substantial variability among the suite of models analyzed and most models simulate circulation patterns more realistically away from influential features such as large bodies of water and complex topography.

Acknowledgements

I sincerely thank all the people who helped make this work possible. First, I'd like to thank my advisor, colleague, and friend Dr. Anthony J. Broccoli. Dr. Broccoli has been my mentor since I was a sophomore in the undergraduate Meteorology Program and has been a loyal and dedicated guide along the way. Dr. Broccoli's patience, and ability to teach the scientific, professional, and personal skills necessary to be a successful scientist cannot be understated.

I would also like to thank the rest of my committee. Dr. Benjamin Lintner has been a supportive and influential mentor and colleague both professionally and personally. I thank Dr. Gabriel Lau for his helpful comments on this work as it progressed as well as his involvement in my educational progress and job search. I largely owe my presence in this department to Dr. Steven Decker as he hired me as his teaching assistant for my first three years. The three years of interacting with undergraduates and learning from Dr. Decker's teaching skills was an invaluable educational experience.

I'd like to thank Justin Sheffield for providing the VIC data used in Chapter 3 and Anthony DeAngelis and Matthew Niznik for aiding in the task of downloading CMIP5 data.

I owe a great deal of thanks to my friend and colleague Dr. Virendra Ghate who helped me tremendously with my work and was a loyal friend and supporter.

I thank the faculty and staff of the Rutgers University Environmental Science Department for their help and service throughout my time here.

Last, but certainly not least, I want to thank the amazing support of my family. The support and patience from my wife, Natasha Hodas, has been invaluable. I am also deeply grateful for the support of my parents. They have instilled in me a desire to learn, to work hard to achieve my goals, and always encouraged me to be curious and follow my interests. Without this upbringing and support I would not have pursued and completed this degree.

Table of Contents

List of Tables

List of Illustrations

Chapter 1

Introduction and Review of Relevant Literature

1.1. Scientific Goals and Motivation

Temperature extremes are associated with severe impacts on both human society and the natural environment with extreme heat in the summer and extreme cold in the winter associated with the majority of climate impacts. As a result of anthropogenic global warming, changes in the severity, frequency, and duration of extreme events are expected. Warm extremes are expected to become more common and occur in places not currently accustomed to or prepared for such events, while cold extremes are generally expected to become less frequent and less severe. Because of the substantial impacts such changes will have on society, it is important to gain a comprehensive understanding of the atmospheric and physical mechanisms associated with these events in order to be better equipped to interpret future projections made by climate models.

This work aims to answer the following broad scientific questions:

1. What are the circulation patterns associated with extreme temperature days over North America and how do their characteristics change with season and location?

To answer this question, several novel metrics were developed that systematically identify and describe these patterns across the entire continent. Patterns were identified as atmospheric circulation anomalies composited for all days that had extreme temperatures. These metrics provide information about the orientation and strength of

the circulation patterns as well as other characteristics such as the degree to which these anomaly pattern scale with temperature. By answering this question, a comprehensive understanding of important mechanisms associated with extreme events is gained and this information will provide a framework for evaluating climate model simulations of extreme events and their associated circulation patterns.

2. How influential are large-scale recurrent modes of climate variability on extreme temperatures?

The associations between extreme temperature days and months and the Pacific North American (PNA) pattern, the Northern Annular Mode (NAM), and the El Niño-Southern Oscillation (ENSO) are quantified for the entire continent. These three patterns are associated with characteristic temperature teleconnections over North America; however, this analysis puts into perspective the relative influence from these modes of variability in relation to smaller-scale, transient weather disturbances and other physical processes.

3. How well do state of the art climate models simulate the observed patterns associated with temperature extremes over North America?

A suite of seventeen general circulation models (GCMs) is systematically evaluated by determining the ability of the models to simulate the metrics devised to describe circulation patterns associated with extreme temperature days from observations (Question 1). This is an important step towards constraining uncertainty in the ability of climate models to simulate changes in future temperature extremes due to global warming. All model output is from the fifth phase of the Coupled Model

Intercomparison Project (CMIP5) created for use by the United Nations Intergovernmental Panel on Climate Change's forthcoming Fifth Assessment Report.

The subsequent chapters of this dissertation address each of the above questions in sequence. The final chapter provides a summary of results and conclusions as well as a discussion of broader implications for science and society. It also concludes with a discussion limitations, unanswered questions, and potential future work resulting from this project.

1.2 Temperature Extremes in the Current and Future Climates

Several recent, high-profile extreme temperature events have demonstrated the danger such events pose to humans. Events like the 2003 European heat wave are expected to become more common in the future (e.g. Beniston 2004, Schär et al. 2004, Stott et al. 2004). Dole et al. (2011) suggest the 2010 Russian heat wave was mostly a result of natural variability while Rahmstorf and Coumou (2011) suggest it was the result of anthropogenic global warming. Otto et al. (2012) argue that the event was a result of a combination of natural and anthropogenic causes. More recently, extreme heat coupled with unusually dry conditions has severely impacted much of the Continental United States in the summers of 2011 and 2012.

Indices of extreme events have been devised and evaluated and consistently show a warming of nighttime temperatures and fewer extreme cold events on global and regional scales (Frich et al. 2002, Alexander et al. 2006, Griffiths and Bradley 2008, Brown et al. 2010). Donat and Alexander (2012) show that the probability density function of daily

temperature has warmed, further confirming the observed increase in warm extremes and decrease in cold extremes globally. Hegerl et al. (2004) suggest that detection of changes in mean temperature cannot be substituted for changes in extremes for most parts of the world. Recent studies using observations and model simulations suggest that the detected warming trend in warm nights (Morak et al, 2011) and extreme warm daytime temperatures (Christidis et al. 2011) is at least partially attributable to anthropogenic external forcing. Rowe and Derry (2012) show that the frequency of record warm temperatures has been increasing while the occurrence of record cold temperature has been decreasing across the continental United States in recent years.

Extreme value statistics have been used to show global and regional changes in observed temperature extremes (Brown et al 2008) and evidence suggests an anthropogenic signal in these changes (Zwiers et al. 2011). Extreme value statistics have also been applied to general circulation model (GCM) simulations and show an overall warming in extremes with the warming on the cold tail being of the greatest magnitude in recent years (Kharin and Zwiers 2000, Kharin and Zwiers 2005, Kharin et al. 2007).

Temperature extremes are expected to change in severity, frequency, and duration as a result of anthropogenic global warming with an increase in warm events and a decrease in cold events likely, resulting from a further shift in the temperature frequency distribution toward higher values (Easterling et al. 2000, Meehl and Tebaldi 2004, Tebaldi et al. 2006, Meehl et al. 2007). Such changes would leave the population of the world vulnerable to extremes that it is not prepared to deal with and in many locations has never experienced before (Meehl et al. 2009). Tebaldi et al. (2006), using general circulation model (GCM) simulations of extreme temperature indices from a suite of

models, show that models project a continuation of the trends in increasing occurrence of warm extremes and decreases in cold extremes that have already been observed. As a result of changes in circulation, there is evidence of regions where extreme cold events may not become less common and in some cases will occur with greater frequency (Vavrus et al. 2004, Kodra et al. 2011).

1.3 Temperature Extremes and Large-Scale Modes of Natural Climate Variability

Anomalous, synoptic-scale circulation patterns have been associated with unusual and extreme temperature events in many cases. Strong circulation anomalies at 500 hPa have been linked to extreme warm temperature events (Meehl and Tebaldi 2004). Cassano et al. (2011) showed the strong associations with preferred circulation patterns and anomalous temperatures over Alaska.

Several recurrent modes of natural climate variability are associated with characteristic teleconnections that impact regional mean temperature over North America, especially in the winter. The Pacific North American (PNA) pattern is associated with geopotential height anomaly centers southwest of the Aleutian Islands, inland of the Pacific Northwest, and over the southeastern United States which correspond to temperature anomalies of the same sign (Wallace and Gutzler 1981, Barnston and Livezey 1987). The Northern Annual Mode (NAM), also referred to as the Arctic Oscillation, is characterized by an annular structure of latitudinally stratified geopotential height anomalies of opposing sign with one band at high northern latitudes and the other over the mid-latitudes. When the NAM is in the positive phase, the mid-latitude westerlies are

anomalously strong, preventing surges of cold air from penetrating southward into the continental United States. This corresponds to anomalously warm temperatures in the mid-latitudes and anomalously cold temperatures in the Arctic. A similar pattern, but with anomalies opposite in sign, is experienced when the NAM is in the negative phase (Thompson and Wallace 1998, Thompson and Wallace 2000, Thompson and Wallace 2001).

The El Niño-Southern Oscillation (ENSO) phenomenon has well documented associations with regional temperature impacts across the mid-latitudes including over North America (e.g. Horel and Wallace 1981, Ropelewski and Halpert 1986, 1987, Kiladis and Diaz 1989, Gershunov and Barnett 1998). Two different types of El Niño events have been identified, each with different temperature teleconnections over North America. The traditional warm event is characterized by warm sea surface temperature anomalies centered over the eastern tropical Pacific (EP) while the other type is centered over the central tropical Pacific (CP) (Yu et al. 2012 and references therein). The temperature anomalies associated with the CP events are associated with a temperature anomaly dipole with warm anomalies over the northwestern United States and cold anomalies over the southeastern United States. The EP events are characterized by warm anomalies primarily over the northern tier of the United States. It is likely that each type of El Niño event influences temperature extremes differently as well.

Several studies suggest a strong linkage between the amplitude and phase of these recurrent circulation patterns and extreme temperatures. Significant impacts on temperature extremes are found by Higgins et al. (2002) due to changes in the phase of ENSO and the NAM across the United States. Gershunov and Barnett (1998) show that

changes in the probability of extreme temperature days in winter over the continental United States due to the phase of ENSO do not necessarily follow systematic shifts in the temperature frequency distribution, characteristic of ENSO. Kenyon and Hegerl (2008) also show statistically significant associations between phases of ENSO and extreme temperature days. Both of these studies show substantial nonlinearity in the response of temperature extremes to opposing phases of ENSO. Recent unusually cold winters over North America and Europe (2009-2010 and 2010-2011) have been associated with a strong negative phase of the North Atlantic Oscillation (NAO, which is highly correlated with the NAM), suggesting a relationship between the amplitude of the pattern and the magnitude of the temperature anomalies (Guirguis et al. 2011, Wang et al. 2010, Cattiaux et al. 2010).

Particular focus from several studies has been given to the association between modes of climate variability and temperature extremes in the northeastern United States and southeastern Canada. Wettstein and Mearns (2002) show a north-south dipole in the sign of the association between temperature extremes and the phase of the NAO/NAM over this region. Griffiths and Bradley (2007) show that extreme warm temperatures preferentially occur during a positive phase of the AO and extreme cold temperatures during a negative phase. Brown et al. (2010) suggest, however, that the influence on extremes from modes of climate variability over long time periods is not robust in this region.

Chapter 2

Characteristics of Observed Atmospheric Circulation Patterns Associated with Temperature Extremes over North America

2.1 Data and Methodology

a) Data

Daily temperature extremes were obtained from the HadGHCND gridded daily temperature data set. The data set is a joint project between the U.K. Met Office Hadley Centre for Climate Prediction and Research and the United States National Climatic Data Center (NCDC). The data set is on a global domain and the majority of the observations that are applied to the gridding process are from NCDC's Global Historical Climatology Network-Daily (GHCND). The resolution of the grid is 2.5 degrees latitude by 3.75 degrees longitude. The data set has two products: gridded observed daily maximum and minimum temperatures which range from 1946 to 2000 and gridded daily maximum and minimum temperature anomalies which range from 1950 to 2007. This work primarily makes use of anomalies which are computed by subtracting the 5 day running mean from a 30 year daily climatology (1961-1990) from the actual temperature. A more detailed description of the data set and the gridding process can be found in Caesar et al. (2006).

Circulation patterns were calculated using data from the National Center for Environmental Prediction's Reanalysis 1 (Kalnay et al. 1996). To calculate anomalies in reanalysis variables the same method and reference period used by Caesar et al. (2006)

was utilized. The resolution of the reanalysis data is higher than the HadGHCND at 2.5 degrees by 2.5 degrees.

b. Methodology

Extreme temperatures were defined as those days where the daily maximum or minimum temperature anomaly was above the 95th or below the 5th percentile in the temperature anomaly frequency distribution for a particular calendar month for the period 1961-1990. This 30 year period was chosen as a compromise between the conflicting goals of maximizing the sample size of extreme events while minimizing the effect of temperature trends in recent decades. The months of January, April, July, and October were analyzed to represent the four standard seasons. Anomalies were used rather than temperature to avoid temporal biases associated with systematic variations in climatological mean temperature during the course of a calendar month; such biases would be acute during the transition seasons. Although warming has occurred during the period of analysis, the extreme events are relatively well-distributed in time and thus the warming did not impact or bias our results in a meaningful way.

The foundation of our results is the analysis of composites of atmospheric circulation variables, with emphasis on anomalies in 500 hPa geopotential height (Z500), and sea level pressure (SLP). Anomalies were calculated by subtracting the five day running mean from a 30 year climatology from the actual SLP or Z500 value for each day. To create the composites, the global anomalies for each of the warmest or coldest days at a particular grid cell were extracted from the reanalysis and then averaged. The sample

size is 47 days for 31-day months and 45 for 30-day months (five percent of 31 (30) days x 30 years) ; however, if there was a tie for the 45th or 47th most extreme day, all days with the same value were included. It is inherent in our method that events consisting of several consecutive days of extreme temperatures were included, thus not all patterns in the composites are fully independent.

To allow for systematic comparison of circulation patterns from different locations, composite patterns were regridded from absolute geographic coordinates to a polar coordinate grid (radial resolution of 250 km and azimuthal resolution of 2°) that is defined in relation to the grid cell at which the temperature extremes occurred. An example of one such "grid-cell relative grid" is shown in Figure 2.1. The outer boundary of the grid is located 4500 km from the central grid cell, a distance that was chosen empirically such that the large-scale and local circulation patterns would be included.

2.2. Composite Analysis

Grid-cell relative composites were developed for all combinations of extremes, seasons and circulation variables, but the bulk of the analysis in this section is focused on extremes occurring in January and July. In the discussion that follows, daily maxima and minima at or below the 5th percentile are denoted by Tx5 and Tn5, respectively, while those at or above the 95th percentile are denoted by Tx95 and Tn95. While January Tx5 and Tn5 (cold winter days/nights) and July Tx95 and Tn95 (warm summer days/nights) are associated with the majority of climate impacts, warm winter extremes (January Tx95 and Tn95) and cold summer extremes (July Tx5 and July Tn5) are also included to

present a comprehensive analysis of the mechanisms associated with days in the tails of the temperature distribution.

a. Description of domain wide patterns

For each type of temperature extreme (i.e., Tx5, Tn5, etc.), composite circulation patterns were computed for each of the 315 grid cells in North America, defined here as all land area north of 17.5° N bounded by the Atlantic and Pacific Oceans on the east and west respectively. The resulting grid-cell relative maps are too numerous to be presented or readily interpreted, thus their content has been summarized by averaging the composite circulation patterns for each type of extreme over the entire analysis domain to produce a "grand composite." Grand composites for each type of extreme are depicted by 2.2, with SLP anomalies indicated by shading and Z500 anomalies by contours. The median value of the pattern correlations between the grand composite and all of the individual composites is provided as a metric of the ability of the grand composite to capture the common features of the individual composites. January extremes are characterized by strong Z500 anomalies (~150 m) located near or slightly to the east of the location experiencing the temperature extreme. The pattern associated with extreme cold maximum temperatures is very similar to that for extreme cold minimum temperatures; however the negative height anomaly center is shifted slightly east in the Tn5 case for January when compared with the Tx5 case. The upstream positive SLP anomaly center also extends closer to the central point in the January Tn5 case. While this shift is subtle and may be due to sampling, it can be understood from a synoptic perspective as

conditions ideal for radiational cooling (calm winds, clear skies) often lead to the coldest nighttime temperatures. In the Tn5 case, the largest positive SLP anomalies are nearly overhead, favoring such conditions, and at Z500 the axis of the trough is slightly downstream, signifying the end of cold advection. Extreme cold maximum temperatures do not have this eastward shift as ongoing advection of the coldest air is still needed to suppress maximum temperatures. Extreme warm January maximum temperatures are characterized by a very strong positive Z500 anomaly and a strong negative SLP anomaly to the west of the grid cell. At the surface this results in a strong southerly component to the flow, which favors warm advection at most locations.

July extremes are associated with weaker anomalies than in January. Northern Hemisphere summer is characterized by a retreat of the westerlies to the north and a weakening of the zonal temperature gradient. This results in less potential for strong, large-scale circulations to develop along temperature gradients that can lead to the advection of anomalous temperatures. The Z500 pattern still has a center of positive (for warm) and negative (for cold) anomalies nearby or downstream, however these anomalies are of smaller magnitude and spatial scale than those seen in January. The shape of the anomalies is also more rounded than in January, likely a result of the fact that unusual perturbations in the Z500 field in the summer are often cutoff from the mean flow unlike the highly amplified ridges and troughs seen in the winter. Additionally, when averaged across the continent, the pattern is more equivalent barotropic in the summer than in winter, when a noticeable upstream oriented vertical tilt is seen between the surface and the Z500 level. in general, the composite patterns are consistent with simple dynamical balance considerations.

Empirical orthogonal function (EOF) analysis was performed on the composite patterns for all 315 grid cells for each type of extreme. In this application, EOF analysis is used to identify spatial covariability across grid cells rather than spatial covariability across time. With the EOF analysis performed in this manner, the variance explained by the first EOF is greatly separated from subsequent EOFs. The patterns for the leading EOF (Figure 2.3) largely resemble the grand composites in Figure 2.2, especially where the variance explained by the first EOF is high. The lower percentage of variance explained in the SLP patterns is indicative of greater spatial variability or a lack of a consistent pattern throughout the domain when compared to the patterns at Z500. The lack of a preferred pattern, especially at the surface, suggests that differing local patterns are being averaged away in computing the grand composite. Pattern correlation coefficients between the first EOF and the grand composite of the corresponding variable and type of extreme are very close to 1 for Z500 and range from 0.6 to 0.9 for SLP for both months. The relative magnitudes of the explained variance resemble the relative magnitudes of median correlation coefficient values in Figure 2.2.

To see where the composite patterns at individual grid cells most resemble the grand composite, pattern correlations between the anomaly pattern at each grid cell and the grand composite are plotted in Figure 2.4. In general, the pattern correlations at Z500 are high, indicating that the local patterns resemble the grand composites. Some exceptions are in the extreme southern extent of the domain, south of the main storm track, with this area expanding northward in July. The atmosphere within this region lacks strong thermal contrasts, resulting in weak and variable circulation patterns associated with extreme temperature days when compared with areas farther north. The pattern

correlations in January in the Rocky Mountains and along the US West Coast are lower for extreme warm minimum temperatures than extreme warm maximum temperatures, indicative of regional differences there. At the surface, SLP anomaly patterns in general do not resemble the grand composites as strongly as at Z500. The lower resemblance suggests more variety in the possible SLP patterns associated with extreme temperature days than at Z500. The resemblance is particularly poor in far northeastern North America in January, and south of the main belt of the westerlies in July where atmospheric baroclinicity is low. In less baroclinic environments, extreme temperatures are less associated with robust large-scale circulation anomalies and more with local processes and surface moisture anomalies as was seen during the 2003 European heat wave (Fischer et al. 2007, Weisheimer et al 2011).

Skewness of the temperature frequency distribution helps identify regions where local circulation patterns are associated with days in the tails of the distribution. Furthermore, the degree of temperature skewness may indicate how sensitive a location will be to changes in extreme temperatures as a result of anthropogenic global warming (Ruff and Neelin 2012). For example, far northeastern North America is both dominated by positive skew (Figure 2.5) and weak or negative correlation with the grand composites. Here a long warm tail is associated with incursions of air from the relatively warm ocean to the east while extremely cold temperatures are associated with a westerly trajectory. This contrasts with locations in the main belt of the westerlies in which the coldest air arrives from the north and the warmest air from the south, leading to a band of low skewness in interior portions of the continent. Farther south, skewness is predominantly negative where infrequent outbreaks of cold air invade a relatively mild region.

b. Variability within composite patterns

Places where the local composites do not resemble the grand composites raise the question: Are the patterns in these areas resulting from distinctly different processes than the areas that do resemble the grand composites, or do these areas lack a preferred circulation pattern associated with temperature extremes? To answer this question, an EOF analysis was performed on the daily anomaly patterns that make up each local composite. The variance explained by the leading EOF of the composite patterns is plotted in Figure 2.6. Locations in which the leading EOF accounts for a higher percentage of variance have more of a preferred pattern associated with temperature extreme days, while lower values of explained variance imply more variability among the circulation anomaly patterns associated with extreme temperature days.

In general, the results from this local EOF analysis do not support the hypothesis that locations in which local composites are poorly correlated with the grand composites lack a preferred circulation pattern associated with temperature extremes. For instance, variance explained by the first EOF is relatively high in northeastern North America despite the weak correlations between the local composites and grand composites evident in Figure 2.4. Thus the lack of similarity between the local composites and the grand composites in that region is likely due to regional differences in the preferred circulation pattern associated with temperature extremes.

More generally, the percentage of variance explained by the leading EOF is higher in January than July and higher for Z500 than SLP. There is a discernible tendency for larger explained variance for warm extremes than cold extremes in January, particularly

for SLP, which may be because warm extremes in winter are more advectively than radiatively driven. An area of relatively high explained variance exists in the central part of the continent associated with extreme cold days in July at the surface, while the same region has relatively low variance explained by the first EOF for Z500. This may be due to cloudiness and precipitation inhibiting the daytime temperature rise during upslope flow events, which are typically confined to the lower troposphere.

c. Pattern symmetry and linearity

Pattern symmetry describes how similar, but opposite in sign, the anomaly patterns associated with cold extremes are to those associated with warm extremes. A metric of pattern symmetry (Figure 2.7) is developed by computing the pattern correlation between the composite pattern associated with extreme cold days and extreme warm days and reversing its sign. Thus a grid cell for which the composite patterns for warm extremes is exactly opposite to the pattern for cold extremes would have a symmetry value of 1.

An additional property of interest is the linearity of the composite patterns. A circulation pattern can be regarded as linear if the pattern for the largest daily temperature anomalies is a higher amplitude version of the pattern associated with smaller temperature anomalies, with the amplitude proportional to the magnitude of the temperature anomaly. A second metric is developed to assess pattern linearity according to the following procedure: For each grid cell over North America, circulation anomalies at all locations in the domain are regressed on the temperature anomaly at that grid cell for all days in the sample. This yields a pattern of regression coefficients that have units of height per

degree (for Z500) or pressure per degree (for SLP). To allow for more interpretable comparisons between these patterns and the composite anomaly patterns determined from the tails of the temperature anomaly distribution, each regression coefficient is multiplied by the mean temperature anomaly for the days comprising the composite, producing a pattern of regression-derived circulation anomalies with the same units as the composites. The RMS difference between each composite anomaly pattern and the regression-derived anomaly pattern, normalized by the standard deviation of the composite anomaly pattern, is then defined as a metric of pattern linearity (Figure 2.8). The pattern linearity would be zero in a case in which the composite anomaly pattern scales linearly in the temperature anomaly. A value of 1 would indicate that the RMS difference between the composite anomaly pattern and the regression-derived anomaly pattern is as large as the spatial variability of the pattern itself, which would be indicative of considerable nonlinearity. Note that symmetry is expressed by one value that compares both the warm and cold composites, whereas linearity is expressed by two values, one each for warm and cold composites.

Circulation patterns are generally more symmetrical and linear at Z500 than at sea level. Both symmetry and linearity are the smallest across the continent in the July SLP cases, which may result from those patterns being less dependent on large-scale circulation patterns and more dependent on local processes and land-surface coupling. Patterns in SLP anomalies associated with cold January days have weaker symmetry and linearity in a band stretching from north-central Canada southeast across Hudson Bay. This indicates that the circulation patterns associated with days in the cold tail of the temperature distribution are different than those associated both with the warm tail and non-extreme

temperature days. This area also correlates to a region of positively skewed temperature distributions (Figure 2.5). SLP patterns have weak symmetry and low linearity values in the US Southwest associated with Tx95 events in January and in the vicinity of the Great Lakes during July extreme warm days. In general, the most symmetrical and linear patterns are found in the main belt of the westerlies, shifting meridionally with the seasons.

d. Spatial scale of patterns

The distance between the center of the greatest positive and negative anomalies in Z500 composite patterns (normalized by the standard deviation of the Z500 anomalies in this case), or the "half-wavelength" of the wave pattern, was calculated for each grid cell. The median distance value was calculated for all grid cells in three latitude bands and plotted in Figure 2.9. With a few exceptions in the lowest latitude band, January has the longest half-wavelength and July has the shortest. The spatial scale of the transition seasons tends toward intermediate values that are larger than July but smaller than January. With a few exceptions, the northernmost band has the longest half-wavelengths and the southernmost has the shortest. There is very little difference between the half-wavelengths of the higher two latitude bands in all cases except for Tx95 where the difference is relatively large. The lowest latitude band (south of 37.5° N) has little or no discernible seasonal cycle in all cases but Tn95. This lack of seasonal cycle may be due to the lesser influence of mid-latitude synoptic-scale systems at lower latitudes. In all cases the half-wavelengths are within the synoptic-scale and smaller in scale than larger-

scale recurrent teleconnection patterns, suggesting that the primary influence on extreme temperature days comes from transient weather patterns.

2.3. Select Cases

The following section examines composite patterns associated with temperature extremes for four different grid cells, each chosen to provide examples of different circulation characteristics as described in the previous section. Each composite is calculated for a specific grid cell; however, the composite patterns can be assumed to be representative of nearby locations.

a. Interior North America: January Z500 Tn5 and Tn95

Figure 2.10 shows maps of the Z500 composite pattern for extreme warm (left) and extreme cold (right) minimum temperature days in January in the far interior of the continent. This is an area characterized by patterns that are relatively linear and symmetrical and a have a strong resemblance to the grand composite for Z500. The extreme warm events are associated with a strong positive anomaly near the location where the extreme temperature is occurring with a ring of negative anomalies surrounding the positive anomaly center. The composite pattern for extremely cold events is similar but opposite in sign. This region is situated such that air trajectories from the colder north and warmer south are unimpeded by terrain and not influenced by large bodies of water. The result is strong symmetry in circulation patterns associated with

days in the tails and patterns that scale with temperature. The composite pattern is larger in spatial scale than the grand composite, yet the local circulation anomalies at Z500 are similar to those seen in the grand composite. The large-scale ridge and trough pattern at Z500 is indicative of a highly amplified wintertime synoptic pattern with little discernible influence from local or regional geography.

b. Central United States: July Tx95 Z500 and SLP

Meehl and Tebaldi (2004) show that anomalous circulation at Z500 was associated with the high impact events of the Chicago heat wave in 1995 and the European heat wave in 2003. Figure 2.11 shows the composite for Z500 and SLP anomalies associated with the warmest five percent of days in the south-central part of the continent. The anomalies in July are weaker than in January, however the anomalies in Z500 and SLP are largely statistically significant at the 5% level (shaded areas in Figure 2.11). At Z500, a positive anomaly is nearly overhead or slightly to the north of the region, which is similar to the pattern that was associated with the 1995 heat wave that affected this region. This implies that the 1995 anomaly pattern is representative of days in the top five percent of the distribution. At the surface, anomalies in SLP are weakly negative across the region.

The variance explained by the first EOF of the patterns contributing to the composites is relatively low at Z500 and correlation with the grand composites is relatively low at Z500 and negative for SLP. The weak anomalies at the surface may indicate that there are other processes, such as low soil moisture content, associated with extreme warm temperature days in this region. The Z500 anomalies are indicative of a wave train, with

other strong anomalies upstream and downstream of the primary positive anomaly center. Lau and Nath (2012) have found a similar wave train pattern in their analysis of North American heat waves.

c. Southwest United States: January SLP Tx5 and Tx95

Figure 2.12 shows SLP anomaly composites associated with extreme warm (left) and cold (right) temperature days in the southwest part of the continent. This is a region characterized by very weak linearity in the Tx95 case and very weak symmetry in the SLP composites associated with extreme warm temperature days. The SLP anomaly pattern that is associated with extreme cold days is characterized by a strong high pressure anomaly to the north and west and a weaker negative anomaly to the south and east. This sets up a strong pressure gradient that allows for surface advection from the north. A slight change in surface wind direction would result in less cold air as advection with a westerly component would have influence from the Pacific Ocean and advection from the interior of the continent would result in advection of desert air rather than air originating in the Arctic.

Extremely warm days in this location are not associated with a localized large scale anomaly pattern in SLP. This suggests that local, smaller-scale processes are likely responsible for extreme warm days in this region, possibly related to topographical features that cannot be resolved at this scale. The greater symmetry and linearity of the patterns associated with extreme warm minimum temperatures suggests that advection on the large-scale is more important for nighttime extreme temperatures.

d. Eastern Alaska: January and April SLP Tx5 and Tx95

In most cases, composites of daily anomaly patterns associated with temperature extremes in the transition seasons (spring and fall) share commonalities with those in the winter and summer; however in this case, unique processes contribute to very different regimes in transition seasons. Figure 2.13 shows composites of SLP associated with extreme maximum temperature days in eastern Alaska and far northwestern Canada. January extreme warm and cold maximum temperatures are associated with relatively high values of symmetry in SLP composites. Following the SLP anomaly contours, anomalous advection of air from the south at the surface is associated with extreme warm days and anomalous advection with an easterly trajectory is associated with extreme cold days. Insolation is negligible in January in this region, leaving surface advection as the primary factor in the occurrence of extreme temperatures. In April, the composite pattern associated with extreme cold days is similar to January, but the pattern associated with extreme warm days is very different. A broad area of positive SLP anomalies is situated over the region with little or no surface wind anomalies. Advection from the south would have marine influence from the relatively cold Pacific and would inhibit the development of a warm airmass. As a result, conditions associated with extreme warm maximum temperature days favor ample sunshine and light winds under high surface pressure.

Composite analysis of total flow (not shown) shows extreme warm temperatures in January associated with a strengthened and expanded Aleutian Low coupled with a strong high pressure center over western North America resulting in a strong pressure SLP

gradient. In April, extreme warm maximum temperatures are associated with a southwestward shift of the Aleutian Low and a high pressure center to the east of the region resulting in weak surface winds and advection. Extreme cold temperatures for both months are associated with a low SLP center to the southeast of the region and high pressure to the north resulting in advection from the relatively cold east and northeast at the surface. The complex interaction between temperature and the trajectory of surface advection and how this changes with season suggests that this is a region in which temperature extremes may be sensitive to relatively modest shifts in circulation. As an example, a circulation anomaly that increases the amount of onshore synoptic-scale flow in this region would likely lessen the number of extreme warm days. While the winter months may not be as sensitive to subtle changes in circulation, April would experience nonlinear changes in temperature extremes under such a hypothetical change in circulation.

Chapter 3

The Influence of Recurrent Modes of Climate Variability on the Occurrence of Extreme Temperatures over North America

3.1. Data and Methods

a. Data

Daily temperature extremes were extracted from the HadGHCND gridded daily temperature data set (Caesar et al. 2006), a joint collaboration between the United Kingdom's Hadley Centre for Climate Prediction and Research's Met Office and the United States National Climatic Data Center (NCDC). The data set has a resolution of 2.5° latitude by 3.75° longitude and consists largely of observations from NCDC's Global Historical Climatology Network-Daily (GHCND). The HadGHCND has two products, observed daily maximum and minimum temperatures, and daily maximum and minimum temperature anomalies. The latter data set, which spans the years 1950-2007, was used. While the HadGHCND has a global domain, only data over North America, defined here as all land north of 17.5 °N between the Pacific and Atlantic Oceans were used. The anomalies are computed by subtracting the five-day running mean from a 30-year climatology spanning 1961-1990 from the actual temperature (Caesar et al. 2006). Composites of circulation patterns were calculated using data from the National Center for Environmental Prediction's Reanalysis 1 (Kalnay et al. 1996) which has a higher resolution than the HadGHCDN data set at 2.5° by 2.5°.

NAM and PNA index values were obtained from the Climate Prediction Center (CPC) website (http://www.cpc.ncep.noaa.gov/). The NAM index is calculated in this data set by projecting the mean 1000 hPa height anomalies on the leading EOF of the 1000 hPa field north of 20° N. The PNA is defined using the first and second rotated empirical orthogonal functions of the 500 hPa geopotential height field following the methods of Barnston and Livezy (1987). Monthly or daily index values are obtained using least squares regression. The Niño 3.4 index data were obtained from the National Center for Atmospheric Research's Climate and Global Dynamics division and are freely available via the web (http://www.cgd.ucar.edu/cas/catalog/climind/Nino_3_3.4_indices.html) and discussed in Trenberth (1997). The Niño 3.4 index is defined as the standard deviation of the monthly sea surface temperature anomaly in the Niño 3.4 region smoothed by a five month running mean. The NAM and PNA are both defined with daily and monthly values while the Niño 3.4 index is only monthly. Daily temperature extremes were therefore associated with the Niño 3.4 index value of the month in which the extreme day occurred. This is a reasonable approximation because the SST anomalies that define ENSO evolve more slowly than the other two modes of variability. In the case of missing index value data, the missing days are removed both from the index values data set and the temperature anomaly data set. This was only an issue for a few days for the NAM in JJA.

b. Methodology

Temperature extremes and composites of circulation anomalies are defined largely in the manner of Loikith and Broccoli (2012) (LB12 from now on) (see Chapter 2) except that a slightly different threshold is used. Extreme temperature days in this work are defined as those days or months falling above the 90^{th} and below the 10^{th} percentile in the temperature anomaly frequency distribution for the months of December, January, and February (DJF) and June, July, and August (JJA) representing boreal winter and summer respectively. The results presented in LB12 (see Chapter 2) indicate that circulation patterns associated with extremes in transition seasons had commonalities with both summer and winter so fall and spring associations are not presented in this paper. The sample size was expanded from that used in LB12 (see Chapter 2) to include three-month data sets and the percentile threshold defining an extreme was expanded by 5% to increase the sample size for evaluating the association between extreme temperature months and the modes of variability. Daily DJF and JJA cold and warm extremes consist of 270 and 276 days respectively for each extreme (90 days (DJF) or 92 days (JJA) per year x 30 years x .10). Monthly extremes consist of nine months for both DJF and JJA (3 months per year x 30 years x .10). The sample size is larger in the case of a tie with the 270^{th} (276^{th}) most extreme day or 9^{th} most extreme month. Analysis was performed using the years 1961-1990 (DJF is December 1960 through February 1990 to keep seasons coherent) chosen as a compromise between the need for a sample size large enough to evaluate significance while attempting to reduce any long-term trend in temperature during the period of analysis.

The associations between extreme temperature days and the phase of each circulation mode was identified by calculating the percentage of extreme temperature events (i.e.,

warm and cold daily and monthly maximum and minimum temperature extremes) that were concurrent with an unusually amplified phase of a given mode. Unusually amplified index values are defined as those falling in the upper or lower quartiles of the distribution of index values. These thresholds were chosen so that the half of index values that are furthest from zero are used and the other half is not. Thus the expected percentage that would occur by chance is 25%. A percentile threshold was chosen as opposed to an index value threshold to equally represent the low and high tails of the distribution of index values, even in the case of a non-Gaussian distribution. This allows us to compare days and months where the temperature and the index value of a given mode are both occurring at the tails of the respective distributions.

Extreme temperature days often occur in series of consecutive days, so each extreme is not necessarily independent. To assess statistical significance without assuming that the data are free of serial correlation, a Monte Carlo simulation was performed. The simulation is performed following this example: The 30-year time series of temperature and circulation index values were divided into 30 individual one-year time series for each of the two variables. Next, the time series are randomly paired and the analysis described in the previous paragraph is performed. This process was repeated 10,000 times, producing a frequency distribution for the association between temperature and circulation index for randomly paired time series. The 5^{th} and 95^{th} percentiles of this synthetic frequency distribution are used as thresholds of statistical significance at the 5% level. This process was repeated for all three modes and for all types of temperature extremes (warm and cold, minimum and maximum) separately so that all association calculations have a confidence threshold for each grid cell.

3.2. Temperature Extreme-Circulation Index Associations

In this section daily and monthly statistical associations between extreme temperatures and the NAM, PNA, and ENSO are presented. A closer look at individual cases is also taken to investigate the influence of these circulation patterns at specific locations versus other mechanisms that may be important for the occurrence of extreme temperatures. Results for the NAM and PNA are presented separately from the ENSO analysis because the NAM and PNA are defined by anomalies in atmospheric circulation while the ENSO index is indicative of the state of the ocean and less directly related to atmospheric circulation. Results are presented for daily and monthly associations between the warmest and coldest 10% of temperatures and the highest and lowest quartiles of circulation index values. (Results from the same analysis with different thresholds do not yield appreciable differences in the pattern and significance of association percentage values.) While associations of all types of extremes in both seasons are computed, for brevity only DJF extreme cold minimum and JJA extreme warm maximum events are presented here as these extremes account for the most severe climate impacts. From this point on, the use of a plus sign as a suffix (e.g., NAM+, PNA+) indicates days when the index values are in the upper quartile (i.e., large positive) and a minus sign (e.g., NAM-, PNA-) indicates index values that are in the lower quartile (i.e., large negative). Temperature extremes are labeled as Tx90 and Tn10 for extreme warm maximum and cold minimum daily temperatures respectively.

a. Statistical Associations

1) PNA and NAM

The percentage of extreme temperature days concurrent with days in the upper and lower quartiles for the NAM and PNA are plotted in Figure 3.1. While a given grid cell could have an association percentage value that is lower than expected by chance (25%), only associations higher than this value that are also significant at the 5% level are shaded. This method shows areas where there is an increased probability of extreme temperatures when the index value is outside of the indicated threshold. The color scheme is such that cold colors are used in conjunction with locations that have an increased probability of extreme cold temperatures during the indicated phase of the circulation pattern while warm colors represent grid cells where there is an increased probability of extreme warm temperatures. The patterns of association values generally correspond closely with those expected from the characteristic circulation anomaly patterns defining these two modes of variability.

The PNA has the most robust association in DJF with a strong increase in the probability of extreme cold minimum temperatures over much of the western and northwestern portions of the continent during negative PNA events. Positive PNA events tend to favor extreme cold temperatures over southeastern North America. These areas of increased probability tend to have decreased probabilities when the sign of the PNA is opposite that associated with the extremes (i.e. PNA- over southeast North America, not shown). Both the northwest and southeast portions of North America are located in the vicinity of the characteristic centers of action that define the PNA. The relatively higher association

values found over northwestern North America in the PNA- case when compared with southeastern North America in the PNA+ case is likely a result of the tendency for the geopotential height anomalies associated with the PNA to be stronger near northwest North America than over southeast North America. In southeastern North America, while a significant increase in the probability of extreme cold minimum temperatures is associated with highly positive PNA days, many such days (~50%) occur when the PNA is not exceeding this threshold. This suggests that the PNA, while an important influence on local daily temperature, is only partially influential for this region.

A positive NAM is associated with an increase in the probability of extreme cold minimum temperatures over the far northeast and northwest portions of the continent where the positive phase of the NAM is associated with lower than average geopotential heights. The area of increased probability of cold events is shifted southward during negative NAM days as a weakening of the prevailing westerlies associated with the negative phase of the NAM allows colder air to penetrate equatorward. The increased probability is much lower for the NAM compared with the PNA and suggests that the NAM may not be a dominant influence in extreme daily temperatures over North America. Some of the area in southeast North America that is associated with NAM- days is also associated with PNA+ days. This indicates that this region is subject to a relatively high influence from large-scale circulation and concurrence of modes could also be important here.

Summertime associations are weaker in general, especially at lower latitudes where weak baroclinicity results in circulation patterns that are smaller in scale and weaker in magnitude than in the winter, as discussed in Chapter 2. There is an increased probability

for extreme warm days over much of Alaska and northwestern Canada during both PNA+ and NAM- events. Similarly, the east-central portion of the continent has an increased probability of extreme warm days during PNA- and NAM+ days. The NAM associations in the summer still suggest an annular structure with a zonal band of significant association values across much of the continent during NAM+ days. The southeast North America area of association that would be expected for the PNA- case based on the results of DJF is not present as this is likely too far south to be strongly influenced by extra-tropical circulation.

Because these patterns evolve and persist over multiple days, it is of interest to examine the association between extremes in both temperature and index value on longer timescales. Figure 3.2 shows the same analysis, except the associations are between extremely warm and cold months and unusually positive or negative index value months. In winter, the patterns are generally similar to those in Figure 3.1 except the percentages are generally higher. Nearly all months with extremely cold mean minimum temperature values occur during PNA- months over much of northwest North America, while the same is true in southeastern North America for PNA+ months. The NAM has similarities with the daily associations, but with stronger percentages for NAM+ over northeast North America and more areas of significant association that are more scattered for NAM-. Some of this scatter may be due to the relatively small sample size of months that exceed the temperature and index value threshold compared with the daily analysis.

Months with extreme warm mean maximum temperature in JJA have some commonalities with the daily associations, especially over northeastern North America for the PNA- case, Alaska for the NAM- case, and eastern Canada for the NAM+ case.

There are few significant associations with PNA+ months when compared with the other association maps. The interior of the northern half of the continent is strongly associated with NAM+ months while only the southern half of this region is present in the daily analysis which could suggest more influence on temperature extremes over longer time scales from the NAM in north-central Canada.

Figure 3.3 shows the percentage of extreme temperature days that occur when neither the PNA nor the NAM exceed the 25% threshold on either end of the distribution. For a day to be counted in this analysis, it must not be concurrent with unusually positive or negative index values for either mode. In this case, all associations greater than 25% are plotted and significant grid cells are highlighted. Most of the domain does not have a significant association percentage when either phase is not in the upper nor the lower quartile and even fewer locations have significantly increased probability in DJF. The results here do suggest, however, that there are numerous days, especially in the summer, when extremes occur when the index value for either pattern is in the upper or lower quartile. While these patterns, and their amplitude may be important in many locations, many extremes do occur when the index values are between the lower and upper quartile of the index value distribution.

2) ENSO

Figure 3.4 shows the associations between extreme temperature events and ENSO for both daily and monthly time scales. In these maps, shading indicates associations that are stronger than would be expected by chance irrespective of statistical significance, while

those grid cells with statistically significant relationships at the 5% level are highlighted. Overall, associations are weak, and the area of statistical significance is much less than that seen in the PNA and NAM cases. The relative weakness of the relationship between extreme temperature events and ENSO as contrasted with the results for NAM and PNA is likely due to the more direct relationship between temperature and local atmospheric circulation. Although ENSO teleconnections clearly affect atmospheric circulation, the influence on temperature is less direct than that of the other two patterns, which are defined by atmospheric circulation anomalies directly over North America. There is an increased probability of extreme cold days over much of the northern and western portions of the continent during La Niña events, but only a few grid cells in Alaska are statistically significant. Associations are generally weak for NINO+ days and months while Alaska has more statistically significance in NINO- months. There is also an increased probability of extreme cold minimum temperature months over the Rocky Mountains and over northeastern North America during NINO- months.

In JJA, the northern tier of the continent shows significantly increased probabilities of extremely warm days and months during La Niña events while Alaska tends to have an increased probability during El Niño months. NINO+ days and months are also associated with an increased probability of warm summer days and months over Mexico and the south-central United States. Places where ENSO is associated with extreme warm temperatures in the summer, especially at lower latitudes, may experience circulation patterns that inhibit precipitation and cloudiness rather than circulation that influences advection of warm air.

Kenyon and Hegerl (2008) show statistically significant associations between the sign of ENSO and extreme temperature days using station data over North America while our results do not show significant associations to be as widespread for the same types of extremes. Our results do show associations of similar magnitude (generally within 5-10% of the expected value), but these locations are not significant according to the Monte Carlo tests employed in this study. One difference in the design of this study that could explain this difference is the smaller sample size of our dataset. Kenyon and Hegerl (2008) used ENSO data ranging from 1849 to 2005 while this work uses 1961-1990. The percentage anomalies found by Kenyon and Hegerl (2008) are relatively small, so a larger data set would be required to find statistical significance with such subtle deviations from expected values. It is also possible that the effects of ENSO on extreme temperatures were weaker during the 30-year period examined in this work when compared with other periods due to variability in the ENSO-associated circulation patterns over North America amongst warm (upper quartile) and cold (lower quartile) events.

3) INDIVIDUAL CASES

Individual locations were chosen to comprehensively examine the interaction between temperature extremes and the modes of variability. Here we present results from four locations represented by grid cells located in Alaska, the United States central Gulf Coast, Baffin Island, and the Great Lakes. Extreme temperatures at the Alaska location are strongly influenced by the PNA and to a lesser extent ENSO. Extremes in the

vicinity of the Gulf Coast are influenced by the PNA and the NAM while Baffin Island is affected by the NAM and the Great Lakes is an example of a location not within a major region of influence from any mode. The Alaska, Gulf Coast, and Baffin Island cases are examples of associations that are stronger than the majority of the continent while results from the Great Lakes location are more representative of areas outside of the main regions of influence from these patterns.

Figure 3.5 shows the index values for all extreme DJF and JJA days and months at the four locations using a box-and-whisker format with each dot representing one extreme temperature day/month. For the daily case, a large spread of index values, regardless of association value or significance, is evident for both modes. Locations where the boxes (outlining the days/months between the 25^{th} and 75^{th} percentile) do not overlap are indicative of cases where the association with temperature is relatively strong. Some notably strong associations with daily extremes, such as Baffin Island with the NAM and Alaska with the PNA, do not have overlap between the boxes while there is still substantial overlap between the dots. Even where there is a preferential phase associated with a type of extreme, it is possible to get an extreme with the opposite phase of the mode.

The Baffin Island case exhibits some asymmetry as the NAM values for daily Tx90 deviate from zero in the negative direction with greater magnitude (median -1.5) than the values for daily Tx10 (median .14) in the positive direction. Only the Baffin Island daily Tx90 NAM case and the Alaska daily Tx90 and Tx10 PNA cases have boxes that fall entirely within one phase of the mode. This ubiquitous spread in daily cases further indicates that extreme daily temperatures are strongly influenced by mechanisms other

than the phase and strength of these modes of variability, even where the NAM and PNA are highly influential on mean temperature or significantly associated with extreme temperature in a statistical sense.

Monthly extremes show less overlap between boxes and in the cases of Baffin Island with the NAM and Alaska with the PNA, there is no overlap between extreme months. There a greater tendency towards a positive phase of the NAM for Baffin Island with monthly than daily Tx10 , but the deviation from zero is still higher for monthly Tx90 indicating some asymmetry at monthly timescales as well. The Gulf Coast location shows strong tendencies towards opposing phases of the NAM and the PNA for extreme months while this is not the case for daily extremes. The Great Lakes location also shows association with the phase of the NAM which is not present with daily extremes. This suggests that the influence from the NAM on temperature at this location is present at monthly timescales while other mechanisms are more important for daily extremes. Plotted in the same manner, JJA box-and-whisker plots show little or no tendency towards either positive or negative phases of either mode for daily or monthly extremes.

The scatter plots in Figure 3.6 illustrate the relationship between minimum temperature and index value for every day in the 30-year climatology at Baffin Island and Alaska in DJF. These are two places where the associations are among the strongest in the continent for both daily and monthly extremes; however, the daily scatter plots show many extreme days that occur when the modes are not in an NAM+/- or PNA+/- state. Overall, there is a relationship between temperature and the phase and strength of the modes as indicated by the slope of the scatter plot, but even locations with the strongest associations in North America still have many extreme days occurring outside of the

index value threshold and in some cases during phases opposite in sign to the preferred phase of association.

The Baffin Island daily scatter plot illustrates the asymmetry seen in the box and whisker plots. The temperature probability density function for this region (not shown) has a long warm tail, largely associated with a negative phase of the NAM, which allows advection of relatively mild marine air from the south and southeast into this relatively cold location. Days in the cold tail are less associated with a preferred mechanism that can cause outbreaks of equally cold air because this location is already in close proximity to the climatologically coldest regions in the hemisphere.

Monthly scatter plots are narrower in shape and have few extreme months occurring during an opposing sign from the mean association than for the daily case. For example, there are some Tx10 days that occur with NAM- months while the majority Tx10 months occur with NAM+ months. In the daily case there are more Tx10 days falling outside of NAM+ days, and even some with NAM- days than in the monthly case. This is also true for the PNA Alaska case as very few months occur with an index value that is outside of the expected phase. The longer time scale increases the association in these two places in a manner that is consistent with the difference between the daily and monthly percentage values depicted in Figures 3.1 and 3.2.

Figure 3.7 shows scatter plots for ENSO DJF minimum temperature associations at the Gulf Coast and Alaska locations, which both are in regions known to be influenced by ENSO teleconnections. These are locations where the associations with ENSO are expected to be stronger than for the majority of the continent. Daily temperatures show

very little relationship with the sign and strength of the Niño 3.4 index while there is a somewhat stronger relationship with monthly temperature. In comparison with the scatter plots for the NAM and PNA, the relationships are notably weak with ENSO in these two locations. There is an apparent tendency for extreme warm months to be associated with La Niña events in the Gulf Coast region with a weaker tendency for extreme cold events to be associated with El Niño events. These scatter plots help illustrate the weak influence ENSO has on the tails of the temperature distribution over North America and suggest that other mechanisms are substantially more important for the occurrence of extreme temperatures especially on daily timescales.

3.3. Other mechanisms

a. Composite analysis

In LB12 (see Chapter 2), composite analysis was used to identify and describe the key circulation anomaly patterns in sea level pressure (SLP) and 500 hPa geopotential height (Z500) associated with temperature extremes over North America. Here a similar technique is utilized, however days preceding and following each extreme day were also added to the composite to investigate circulation anomalies that occur on longer timescales than that characteristic of weather. This technique allows the signal of modes of climate variability to diverge from patterns caused by transient, shorter-lived weather events. Figures 3.8 and 3.9 show maps where the anomalies for Z500 and SLP for the day of the extreme (labeled ±0) are composited and maps where the seven days before and after (labeled ±7), including the day of the extreme, are composited. The sample size

of days used to compute the composite is consequently 15 times higher for the ±7 day composites and can include the same day multiple times in the case that 15-day windows overlap. All DJF plots are for extreme cold minimum temperature days and all JJA plots are for extreme warm maximum temperature days.

The ±0 composites for cold minimum temperature days in DJF show robust negative Z500 height anomalies nearby or downstream of the location with weaker positive anomalies upstream. The pattern of height anomalies resembles the characteristic wave train associated with the positive phase of the PNA for the Gulf Coast example and the negative phase of the PNA for the Alaska example. When the composite includes the entire 15-day period centered on the extreme day, the local anomaly center weakens in greater proportion to the anomaly centers further away while maintaining the PNA-like wave train. A disproportional weakening of the local anomaly center in relation to the more remote anomalies is suggestive of the larger-scale teleconnection pattern playing an important role as local synoptic-scale weather events are averaged out. The local anomaly pattern in the ±0 day composites can therefore be considered a combination of a larger-scale circulation pattern like the NAM or PNA and local weather that contribute together to cause an extreme temperature day. In the Alaska and Gulf Coast cases, the PNA may acts as an important factor in the occurrence of extreme temperature days, but local weather plays a role in determining which specific days breach the 10% temperature threshold. A similar result is seen at Baffin Island, except with the positive phase of the NAM. The Great Lakes example exhibits some commonalities with the negative phase of the NAM but with a very strong weakening of the local negative anomaly center, weather likely plays a strong role in this region. The SLP anomaly plots in Figure 3.9

further support the hypothesis that a local weather pattern being superimposed on a teleconnection patterns is highly associated with extreme temperature days in these locations. The SLP patterns weaken considerably in the composites of the 15-day periods, especially at lower latitudes. For example, the Alaska SLP anomaly is associated with the Aleutian Low rather than surface pressure systems propagating with the prevailing westerlies that are more common at the Great Lakes and Gulf Coast locations.

In JJA, Z500 anomalies are weaker, especially at the two lower latitude locations (Gulf Coast and Great Lakes). The weakening of the anomalies in the ±7 day cases is more proportional between all anomaly centers. While this is subtle, it is consistent with a summertime pattern that is dominated by local, smaller scale circulation that often persists for timescales shorter than 15 days. At high latitudes, like in the Alaska and Baffin Island cases, strong anomalies are still present even in the ±7 day case. Here the atmosphere is relatively baroclinic in the summer when compared with lower latitudes so large-scale circulation that evolves over long time periods is still common. SLP anomaly patterns are weaker overall in JJA when compared with DJF and are particularly weak at the Gulf Coast and Great Lakes locations. In the ±7 day cases, the anomaly patterns become weak to nearly non-existent in all cases. These results support the lower association percentages seen in JJA and are consistent with the overall weaker atmospheric circulation in the Northern Hemisphere summer months.

b. Anomalous soil moisture and JJA extremes

The weaker association percentages and lack of evidence of large-scale circulation patterns in JJA lead to a question: If large-scale, recurrent modes of climate variability are not highly associated with extreme temperatures in the summer, what other mechanisms are important? One possible mechanism is anomalous near-surface soil moisture content. To test the hypothesis that extreme temperatures in the summer are strongly associated with anomalous soil moisture, Figure 3.10 shows the association percentages between extreme warm JJA maximum and minimum temperature days and extremely dry soil moisture (lower quartile of days) and extreme cool JJA maximum and minimum temperature days with unusually moist soil (upper quartile of days).

Soil moisture reanalysis data used here is a product of the Variable Infiltration Capacity (VIC) model (Liang et al. 1994) and is available for the continental United States for the time period and resolution needed for this analysis. The limited spatial coverage is sufficient for this analysis as areas north of this region are more influenced by synoptic-scale circulation patterns in the summer than the continental United States while only a small fraction of the domain used in this paper lies to the south. The data is originally on a 0.5° by 0.5° grid but was smoothed to a 2.5° by 3.75° grid to match the HadGHCND temperature dataset. Only soil moisture amounts (in mm) for the topmost soil layer were used to calculate soil moisture anomalies. Anomalies were calculated relative to normal values for each day obtained using a 5-day window centered on each day of a 30-year climatology for each day. Anomalies are expressed as percentage of normal soil moisture for each grid cell in the domain.

In almost all locations, extreme warm maximum temperature days have a higher probability of occurring when soil moisture is unusually low. This is consistent with the

expected association as dry soil can enhance surface temperatures due to decreased evaporation and evapotranspiration and has been associated with extreme heat episodes like the European heat wave of 2003 (e.g. Fischer et al. 2007). Extreme warm minimum temperature days are less associated with unusually dry conditions. Because minimum temperatures occur during the night when there is no insolation, dry surface conditions would not be expected to enhance heating or inhibit cooling. Areas where there is a significant increase in the probability of extremely warm nights when soil moisture is low, may be cases where the air mass is extremely hot due in some part to unusually dry soil.

Similar to the enhancement effect on surface temperature that unusually dry surface conditions have, unusually wet soil can inhibit surface heating during the daytime. There is a strong association between extremely cool JJA maximum temperatures and unusually moist soil over the western half of the United States with weaker, but still significant associations along the Gulf Coast. This association could indicate that unusually moist surface conditions inhibit daytime warming, but it could also suggest that weather patterns that cause precipitation in this region decrease the temperature through cloudiness or evaporative cooling of the lower atmospheric column by precipitation. The same association is not seen in extreme cold minimum JJA temperatures where unusually moist surface conditions can dampen diurnal cooling. Additionally, if wet days are associated with cloudiness, this could also inhibit nighttime radiational cooling.

Chapter 4

Comparison between Observed and Model Simulated Atmospheric Circulation Patterns Associated with Extreme Temperature Days over North America using CMIP5 Historical Simulations

4.1. Data and Methodology

a. Data

All model output used in this chapter is from the fifth phase of the Coupled Model Intercomparison Project (CMIP5). This is the latest phase of a coordinated effort by modeling groups worldwide to systematically perform numerous prescribed climate model experiments. The output from the model simulations is archived and available to the scientific community through the Program for Climate Model Diagnosis and Intercomparison (PCMDI). A detailed description of the experimental design is available in Taylor et al. (2012). This work utilizes seventeen individual models from thirteen different modeling groups (Table 4.1). All output used comes from the historical simulation of each model. These are stimulations of the past several decades using observations using observed radiative forcing to use as a control for model evaluation. This work utilized daily maximum and minimum temperature, sea level pressure, and 500 hPa geopotential height from these simulations. Only models with all three of these variables for the historical and two global warming experiments (RCP4.5 and RCP8.5) were used. The requirement for future simulation output is imposed in anticipation of future work that will analyze global warming simulations in comparison with historical

simulations for each model. Geopotential height was provided directly by each model with the exception of the INM-CM4 and GFDL-ESM2G models, for which the hypsometric equation was vertically integrated to calculate 500 hPa geopotential height. All models lacking geopotential height on pressure coordinates or the variables needed to vertically integrate the hypsometric equation were not used in this work.

Daily, observed temperature data was obtained from the HadGHCND gridded daily temperature data set. The data set is a joint project between the U.K. Met Office Hadley Centre for Climate Prediction and Research and the United States National Climatic Data Center (NCDC). The data set is on a global domain and the majority of the observations that are applied to the gridding process are from NCDC's Global Historical Climatology Network-Daily (GHCND). The resolution of the grid is 2.5 degrees latitude by 3.75 degrees longitude. The data set has two products: gridded observed daily maximum and minimum temperatures which range from 1946 to 2000 and gridded daily maximum and minimum temperature anomalies which range from 1950 to 2007. We primarily make use of the anomalies in this work which are computed by subtracting the 5 day running mean from a 30 year daily climatology (1961-1990) from the actual temperature. A more detailed description of the data set and the gridding process can be found in Caesar et al. (2006).

Circulation variables used to calculate observed circulation patterns were obtained from the National Center for Environmental Prediction's Reanalysis 1 (Kalnay et al. 1996). To calculate anomalies for the reanalysis variables utilized, the same method and reference period as Caesar et al. (2006) for the gridded temperature anomalies was used. The same method was applied to the model simulated sea level pressure and geopotential height

output to obtain anomalies, and the model circulation variables were kept on their respective native grid except as indicated for analysis of individual cases. Only data for North America is used, defined here as all land north of 17.5 degrees north latitude, bounded on the east and west by the Atlantic and Pacific Oceans respectively. This equates to 315 grid cells in the analysis domain.

b. Methodology

The methods for calculating circulation anomaly patterns using the CMIP5 data follow the technique used by LB12 (see Chapter 2) where a more detailed description can be found. All model simulated temperature data was regridded to the resolution of the HadGHCND dataset. Because the resolution for each model is finer than that of the HadGHCND data set, an area averaging technique was used in all cases for the regridding process. Anomalies of temperature and circulation variables were calculated in the same manner as the HadGHCND data set and the same 30-year period (1961-1990) was extracted and used to match that used for the observations. Temperature extreme days are defined as those days falling below the 5^{th} and above the 95^{th} percentile in the temperature frequency distribution and extremes were identified for January, April, July, and October.

Following the procedure in LB12, composite patterns of anomalies in SLP and Z500 were computed for days concurrent with extreme temperatures at each grid cell for each model. All composite patterns were then regridded to a grid cell relative grid such that

the center of the domain is the grid cell where the extreme temperatures are identified (see Figure 2.1).

The structure of this paper largely follows that presented in LB12 (see Chapter 2). In the following section, results from a systematic comparison between the model simulated circulation patterns and those computed using observations and reanalysis is presented and the next section looks at individual cases.

4.2. Comparison between Model Simulated and Observed Composite Analysis

This section compares some of the model simulated circulation metrics developed for LB12 (see Chapter 2) with the observed patterns. In most of the analyses, the multi-model ensemble, consisting of the seventeen individual models is presented. Individual models vary in horizontal resolution and physical complexity (Earth system models being highly complex). This variability is associated with a spread in the ability of individual models to simulate these patterns. The technique used in this section aims to summarize the overall ability of the models to simulate the characteristics of observed temperature extremes given the very large number of dimensions inherent in an analysis of so many different data sets and variables.

a. Composite Pattern Correlations

A portrait diagram is used in Figure 4.1 to summarize the ability of each individual model to simulate the composite pattern for each type of extreme. Portrait diagrams are an

efficient way to systematically summarize the results from multi-model analysis (Gleckler et al. 2008). Each model is randomly assigned a letter, labeled on the x-axis. Table A.1 in the appendix identifies the models corresponding to the letters in Figure 4.1. The portrait diagram in Figure 4.1 shows the median values of the set of pattern correlations between the observed composite pattern at each grid cell and the corresponding simulated composite pattern for each model. In general, correlation is very high between the model simulated and observed composite patterns at Z500 in all seasons with lower values for SLP. The higher variability in circulation near the surface is likely the cause of the weaker correlation with SLP patterns when compared with upper level patterns. The weakest correlations are for July Tx5 and Tx95 and April Tx95 when SLP circulation is relatively weak and other factors may be more influential on extreme temperatures.

The maps in Figure 4.1 show examples of individual model results that were used to create the portrait diagram. The map of January Tx95 Z500 for model G is an example of a model that largely correlates well with observations while the July Tx5 Z500 map for model J has a relatively low resemblance to the observations. The January Tx5 SLP example is a “middle of the pack” case that has neither high nor low median correlation in relation to other models. In both of the lower two panels in Figure 4.1, large regional variability in correlation values suggests that models may be able to simulate patterns in some regions realistically while overall having a relatively unrealistic representation continent-wide.

To summarize the circulation patterns for the entire continent (315 different patterns corresponding to each grid cell) a “grand composite” was calculated as in LB12 (see

Chapter 2). The grand composite is the result of compositing each individual composite pattern over the entire domain for a given type of extreme (n=315 for each model). Figure 4.2 shows the grand composites for Z500 and SLP patterns for observations and the multi-model mean. The multi-model mean grand composite patterns resemble the observed grand composites well in both January and July. The models realistically represent the local, strong anomaly at Z500 near the grid cell where the extreme temperatures are occurring as well as the weaker upstream and downstream anomalies. SLP patterns are also well represented by the model mean in both seasons. July Z500 patterns are slightly weaker in the multi-model ensemble grand composite, possibly resulting from more inter-composite variability amongst the models (n=315 grid cells × 17 models).

The titles in Figure 4.2 show the median pattern correlation coefficient when the grand composite is correlated with each individual composite pattern in the North American domain. In this case, the model correlation coefficients in the title are the median values when the 315 model mean composites are correlated with the model mean grand composite. In all cases except July SLP, the multi-model mean composite patterns are more highly correlated with the grand composite than in observations suggesting that the larger number of cases in the multi-model ensemble may average out noise that reduces this value in the observations.

Figure 4.3 shows the correlation of the grand composite of each individual model with the observed grand composite. Each symbol represents one of the seventeen models and the correlation between the ensemble mean grand composite and the observed grand composites is plotted with a large black cross. In all cases, the majority of the models do

not perform as well as the ensemble mean indicating that the process of creating the multi-model mean averages out individual model misrepresentations. Some models perform better than the ensemble mean, although these higher performing models are not consistent amongst all types of extremes. Some models appear to do better with some extremes than others (i.e. blue * is higher than the multi-model ensemble for January Tx5 SLP and relatively low for July Tx95 SLP). There is a much larger spread in the correlation values for July compared with January and for SLP compared with Z500. This is consistent with the findings in LB12 (see Chapter 2) that SLP and summertime patterns are less spatially consistent across the continent and less temporally consistent within a composite.

Figure 4.4 contains maps of the correlations between the composite pattern for each grid cell and the grand composite for observations and the multi-model ensemble. Here, a correlation map was made for each model, then the ensemble mean of the correlation coefficients are plotted in Figure 4.4. The model simulated maps largely resemble the observed maps including regional features in most cases. At Z500, the models capture the relatively high correlation with the grand composite for both January and July and in July the area of weaker correlation in the lower latitudes is also realized in the models. For SLP, much of the regional variability is represented in the models including the area of weak and negative correlation in the southwestern portion of the continent for January Tx95 SLP. In the July SLP cases, the models capture the negative correlation values south of the main track of the westerlies, but do not expand this area far enough north. Also in the July SLP cases, the model values are lower at high latitudes than in observations. This may be related to the ability of the models to simulate the storm track

in summer when baroclinicity is low and synoptic-scale circulation is less dominant, especially south of the main belt of the westerlies.

Figure 4.5 is the same as Figure 4.4 except for two individual models. The left two columns are for a model that resembles the observations relatively well for these cases and the right two columns are for a model that has a less realistic simulation of the observations. Regional discrepancies explain the majority of the differences between the two model simulations. The higher performing model captures the area of negative correlation in the southwestern portion of the continent for January Tx95 SLP while the lower performing model only captures some of the southern extent of this area. The lower performing model has an area of weak and negative correlation with the grand composite over northeastern North America for January Tx95 Z500 while this area has high correlation with the grand composite in observations and the higher performing model. The higher performing model captures the area of negative correlation over the southern portion of the continent better for July SLP, especially for Tx5, when compared with the lower performing model.

b. Temperature Skewness

Figure 4.6 shows maps of observed and multi-model simulated temperature anomaly skewness for North America. The ability of a model to capture the correct skewness of a local temperature probability density function (PDF) is important for realistic simulation of extreme temperature events and can indicate how well the model is simulating the mechanisms associated with days in the tails of the PDF. Places with highly skewed

temperature PDFs are likely associated with a particular mechanism or influence from a temperature controlling region such as a large body of water. If a model does not accurately capture skewness, it is possible that the model does not have realistic mechanisms associated with extreme temperatures in that region.

For January maximum temperatures, the observed and model simulated skewness values are very similar in pattern (i.e. areas of positive and negative skewness match). In general, skewness is negative over the southwestern half to two-thirds of the continent while the remaining portion of the continent has positive skewness. This is captured by the model ensemble and the area dividing the regions of primarily positive and negative skewness is very well captured by the model mean. July skewness is also relatively well simulated in pattern; however there are more areas of disagreement in July than January. The overall positive skewness in the northern half of the continent is not as well captured in the model mean map while the negative skewness in the southern half of the continent is captured by the models.

c. Pattern Symmetry and Linearity

Symmetry describes how similar the composite pattern associated with extreme cold days is to the pattern associated with extreme warm days and is defined as the resulting pattern correlation coefficient when both patterns are correlated (perfect symmetry would have a coefficient of -1 and the patterns would be the same but opposite in sign). Pattern linearity describes how well the patterns scale with temperature. A linear pattern would have a composite pattern associated with extreme temperature days that was a linearly

scaled version of the patterns associated with days that were not extreme. Section 2.2c gives a detailed description of pattern symmetry and linearity and the calculation process.

Figure 4.7 shows both observed and model simulated pattern symmetry with the left column showing observed and the right column showing the median symmetry values of the seventeen models. In this case, the model value at a grid cell is the median symmetry value for all seventeen model simulated symmetry values. In all four cases, the models realize the majority of the features found in observations with the poorest performance being the July SLP case. July SLP patterns are generally small, weak, and highly variable within a composite pattern (LB12), and this increased variability relative to the other cases likely contributes to the weaker representation of the observations.

Some regional characteristics in symmetry are well-captured by the models. The area of weak symmetry over the southwestern portion of the continent (corresponding to the area of negative correlation with the grand composite in Figure 4.4) for the January maximum SLP example is represented by the models but with slightly higher symmetry values. The band of weak symmetry in northern Canada is also represented in the models for January maximum SLP. The area of weak symmetry in the southern portions of the continent for July maximum Z500 is present in the models while July SLP is overall less symmetrical in the model ensemble compared with observations.

Observed linearity and the median linearity of the seventeen models is presented in Figure 4.8 with the observed values in the left two columns and model median values in the right two columns. Linearity shares some commonalities with symmetry because they both describe how the patterns associated with days in the tails relate to each other,

and the median of the seventeen models captures these similarities in many cases. The January Tx95 SLP area of weak linearity in the southwestern region (corresponding to weak January maximum SLP symmetry) is present in the models as is the area of weak linearity in northern Canada in the same maps. As was the case with symmetry, the poorest representation by the models is for July SLP where several regional differences exist. In the July Tx5 SLP case, the area of the Rocky Mountains that has negative values for linearity is not present in the models. The area of weak linearity in the vicinity of the Great Lakes in the July Tx95 SLP case is also not present in the models. These are both areas where complex terrain and proximity to large water bodies can make a substantial difference in surface temperature over short distances. To accurately capture mechanisms for these areas, gridded observations of high resolution or regional model data may be helpful. While other subtle regional variations and disagreements exist, the model median captures the broad linearity features in each case.

4.3. Individual Cases

This section takes a closer look at the composite patterns for four select locations following LB12. Each location was chosen initially in LB12 to present examples from regions with interesting characteristics in circulation patterns associated with extreme temperature days. It is recognized that there are other interesting examples and others were investigated, but these four were chosen to give the best overview of circulation patterns in a concise presentation. For comparison with observations, in all cases the multi-model mean and two individual model results are presented along with the

observed pattern. Model M and P were chosen (names corresponding to those labeled in the portrait diagram in Figure 4.1) as examples of models that generally realize the patterns relatively realistically and unrealistically, respectively. All model simulated Z500 and SLP anomalies have been regridded to 2.5 degrees latitude by 2.5 degrees longitude to match the resolution of the reanalysis data used to calculate the observed patterns.

a. Interior North America: January Z500 Tn5 and Tn95

This region is characterized by strong symmetry and linearity in Z500 circulation patterns in January. The location in the interior of the continent, away from major bodies of water and mountain ranges, contributes to the relative symmetry of the patterns here. Figure 4.9 shows the observed pattern in the top two panels for extreme warm and cold daily minimum temperatures in the vicinity of the highlighted area. Strong Z500 anomaly centers near the region are the dominant feature with positive anomalies corresponding to warm days and negative anomalies corresponding to cold days. There are also upstream and downstream anomalies of opposing sign. The multi-model mean of this pattern, presented in the second row captures most of these features in both the Tn5 and Tn95 cases. The upstream negative anomaly for Tn95 is weaker for the model mean and the upstream positive anomaly is weaker and displaced westward for the Tn5 case. The areas of positive and negative anomalies also appear more circular in the model mean, likely resulting from a reduction of intermodel differences by averaging of the seventeen models.

Model M (third row) resembles both the model mean and the observed pattern well with the simulated pattern for the Tn95 case appearing the most similar to the observations. The local positive anomaly center has anomalies of higher magnitude compared with observations, and the center of the anomalous region is shifted north in Model M. The Tn5 case also shows the local anomaly center shifted slightly north of the observed location with anomalies that are more negative than those observed. The upstream positive anomaly center for Tn5 is displaced to the north and weaker than the observations.

Model P (bottom row) captures the location of the local positive anomaly center for the Tn95 case better than Model M, but the upstream area of negative anomalies is much weaker than in observations. The local area of positive anomalies is also more latitudinally elongated compared with observations. For Tn5, the negative anomaly area is weaker than in observations and stretched out in a northeast to southwest direction rather than the relatively round appearance in observations. Here, the positive anomaly center upstream is much stronger than in observations; however the location of this upstream region of positive anomalies is similar to observations. Overall, the models represent these examples well, which is likely a result of the relative simplicity of the geography and topography of this area (i.e. lack of complex terrain, influential large bodies of water).

b. Central United States: July Tx95 Z500 and SLP

Figure 4.10 shows the composite pattern for a Central United States heatwave in July. The observed pattern shows an area of positive Z500 anomalies with a wave-train of negative and positive anomalies upstream and downstream. SLP anomalies are weak with a broad area of negative SLP anomalies across much of the region. The model-mean for this case captures the local area of positive Z500 anomalies and does show a wave-train upstream and downstream, but the spatial scale of the anomalous ridge-trough pattern is larger than in observations. Some of the anomaly centers in the observed case, especially further away from the region where the extremes are occurring, may have contributions from noise that gets smoothed in the model averaging. This could result in the broader wave-train pattern in the multi-model ensemble. The pattern of SLP anomalies over North America is realistically represented by the ensemble mean.

Model M captures the wave-train pattern and the local anomaly center well at Z500 and even realizes the “double-barrel” structure to the positive anomalies with one center being the local positive anomaly and the second located near Baffin Island. The upstream negative anomaly is simulated realistically with the meridionally stretched features of the anomalous trough present in the model results. The general features of the SLP pattern are also captured, and the small local discrepancies are likely explained by the relatively weak circulation pattern. The model simulated SLP pattern expands the negative SLP anomalies too far north and the model does not have an area of positive SLP anomalies over the far northeastern portion of the continent.

Model P realistically captures the local Z500 anomaly center, but does not have a well-simulated wave-train pattern. The anomalies are, in general, too strong and the anomalous ridges and troughs spatially too large. The SLP pattern for Model P is also

less realistic than in Model M, and has anomaly magnitudes that are too large. It is expected that this case has more variability between models because circulation patterns in July are less consistent within a composite pattern for a given location when compared with winter patterns. The weaker circulation patterns and more variability within a composite at a location in the summer, especially for SLP, should increase the probability that the models do not realistically simulate the patterns for this case. It does appear, however, that the models are able to realize the local anomaly centers relatively well, especially at Z500.

c. Southwest United States: January SLP Tx5 and Tx95

The SLP patterns for extreme maximum temperatures in January in the region highlighted in Figure 4.11 exhibit very weak symmetry and linearity. The observed patterns in the top two rows of Figure 4.11 show the greatly differing mechanisms associated with extreme temperatures here. Extreme warm days are associated with an area of very weak positive anomalies in the vicinity and to the southeast of the region. A broad area of negative SLP anomalies stretches from Alaska across the continent to the Atlantic Ocean. For extreme cold days, a strong area of positive SLP anomalies is present south of the Gulf of Alaska, suggesting a weakening and displacement of the Aleutian Low. There is also an area of negative SLP anomalies to the south and east of the region creating an anomalous pressure gradient promoting advection of air from the colder interior of the continent.

In the multi-model mean, the asymmetrical characteristics of this region are well represented with the most notable difference being a northeastward shift of the positive SLP anomaly over the Gulf of Alaska in the Tx5 case. Model M also captures the overall features of the unusual circulation pattern of this region. The positive anomaly in the Tx5 case is stronger than in observations, but the location and shape of the pattern is realistic. There is an area of positive SLP anomalies over western Alaska in the Tx95 case that is not present in the observations, but this is fairly remote and may not indicate a physically important difference between the model and the observations. Model P also captures the majority of the features seen in the observations but with a similar shift in the Tx5 positive SLP anomaly center to the northeast, similar to the multi-model mean. Considering the complex topography, possible marine influence, and unusually asymmetrical and non-linear characteristics of the circulation patterns for this region the models appear to capture many of the important features with relatively high skill.

d. Eastern Alaska: January and April SLP Tx5 and Tx95

Transition seasons (April and October) generally have similarities with January and July and are therefore not the focus of this paper; however, in some cases circulation patterns in transition seasons are much different from the other seasons. In eastern Alaska, the SLP pattern for Tx95 days is very different from January Tx95 days. Figure 4.12 shows maps for the observed SLP patterns for Tx5 and Tx95 days for April and January in the top row. The SLP patterns for January are highly symmetrical when SLP anomalies promoting advection from the relatively mild ocean contribute to warm extremes and

advection from the relatively cold interior of the continent contributes to cold extremes. In January, insolation is not a factor in surface temperature at this latitude. In April, the Tx5 pattern is similar to the January Tx5 pattern, but the April Tx95 pattern is very different from the Tx5 patterns. In April, the ocean is relatively cold, so advection from the south would inhibit extreme warmth. Insolation is important in April and an area of anomalously high surface pressure is associated with sunny, calm conditions that promote surface warming. The interior of the continent is still relatively cold in April allowing the SLP pattern to look similar to the January pattern.

The multi-model ensemble resembles the observations well for January Tx5 and Tx95 and for April Tx5. April Tx95 does not resemble the observations well with a north-south positive-negative dipole of SLP anomalies appearing to be rotated nearly 90 degrees to the left. The results from model M and P suggest that this discrepancy may be a result from large variability within the model ensemble. Model M captures the orientation of the SLP anomalies well, although the magnitude of the anomalies is generally higher than in observations. This is also the case for the other three columns for Model M. Model P captures the major features of the January Tx5 and Tx95 and April Tx5 cases, but does not resemble the April Tx95 pattern well. The pattern simulated by Model P for April Tx95 would promote advection from the south where the relatively cold ocean would inhibit surface warming at this time of year. It is likely that with the complex topography, influence from land-surface features (i.e. snow and ice cover, vegetation) in this region, this is a difficult area for models to accurately represent.

Chapter 5

Summary, Conclusions, and Implications for Future Work

5.1. Summary and Conclusions

This work, broadly defined, identifies and describes the atmospheric circulation patterns associated with extreme temperatures over North America in both observations and a suite of climate models. Because every location has a unique circulation pattern associated with local temperature extremes, the overarching challenge for this work was to describe these patterns in a way that avoided analyzing and presenting a cumbersome amount of information. To address this challenge, several novel metrics were devised that allow for systematic identification and description of circulation patterns for all of North America. The result of using these metrics was a much more concise summary and description of these patterns across the continent. These metrics are also useful in comparing model simulated circulation patterns to those identified from observations. As a result, this work contributes to the knowledge of meteorology and climatology in two broad ways:

1) Presenting a fundamental, comprehensive analysis of the major circulation patterns associated with extreme temperature days in observations and models.

2) Demonstrating how specialized metrics can be developed and used to systematically describe something as spatially and temporally variable as atmospheric circulation for an entire continent.

a. Summary of Observational Analysis

Observational analysis shows that in general, warm extremes are associated with positive anomalies in the Z500 and SLP field downstream of a location experiencing extreme temperatures with negative anomalies upstream in most cases. Composites of anomalies in Z500 and SLP generally have stronger magnitudes and larger spatial scales in January than in July with the transition seasons reflecting characteristics of both solsticial seasons. Patterns associated with extreme warm and cold days are the most symmetrical and linear at Z500 and in January. Local topographical influences as well as the influence from local land-surface characteristics and proximity to large bodies of water affect the symmetry and linearity of the composite patterns. Locations in the westerlies tend to resemble the pattern obtained when all composite patterns for the entire continent are combined into one "grand composite" better than areas outside of this region, and SLP composites are more spatially variable than Z500. In some cases, regions that do not resemble the grand composite patterns have a preferred, but different composite pattern as indicated by relatively low variability between the daily patterns contributing to the composite. The variance explained by the first EOF of all composite patterns for a given extreme is higher for Z500 than SLP, an indication that circulation patterns aloft are more consistent than at the surface.

The results of this work suggest that some places may be more sensitive to subtle shifts in circulation that could occur as a result of anthropogenic climate change. Expected changes in storm tracks (Yin 2005) and the expansion of the area influenced by tropical

circulation (Lu et al. 2007, Seidel et al. 2008) are both examples of changes in circulation that could yield nonlinear impacts on local temperature. Regions where temperature is strongly influenced by large bodies of water or land-surface conditions (such as the eastern Alaska/northwestern Canada example in section 2.3d) could also experience nonlinear impacts from shifts in circulation or changes in ocean temperature or land-surface characteristics. Regions within the westerlies, where the circulation anomalies associated with extreme temperature days are currently made up of unusually strong weather disturbances, could end up in a less baroclinic environment as the earth warms, resulting in weaker circulation anomalies.

The spatial scales of the Z500 and SLP anomaly patterns generally fall within the synoptic scale. While some patterns visually suggest influence from large-scale teleconnection patterns (not shown), such as the Arctic Oscillation and the Pacific-North American pattern, there is a major influence from local synoptic-scale weather perturbations in each composite pattern, especially at locations within the westerlies. The spatial scales of the circulation patterns tend to be smaller in July as the atmospheric is less baroclinic and extremes are likely influenced by smaller-scale and physical processes not represented in the composites.

The influence of the PNA, NAM, and ENSO on extreme temperature days and months for North American winters and summers has also been quantified. Results suggest that the PNA and NAM play important roles in the occurrence of extreme temperature days in the regions in the vicinity of the characteristic atmospheric circulation anomalies associated with these modes of variability. More extreme temperature days are influenced by the PNA than the NAM over the continent in the winter. Areas in

northwestern North America are strongly influenced by the PNA while the PNA affects southeastern North America in the opposite way in winter. The NAM is also highly influential over the northeastern parts of the continent and in a band running from the northwestern to southeastern parts of North America in the winter. Few locations have an increased probability of extreme temperatures when neither the PNA nor the NAM are unusually positive or negative.

Local, transient, synoptic-scale weather patterns are instrumental in causing a given day to have an extreme temperature in most locations, but this is often in conjunction with an unusually strong phase of an influential mode of climate variability. Composite analysis of anomalies in SLP and Z500 at four locations illustrate the dominance of the PNA and NAM in the areas of influence for these patterns, while also showing that synoptic-scale weather patterns superimposed on these larger-scale teleconnection patterns are present. Summertime associations are weaker and largely limited to higher latitudes where large-scale circulation is more dominant compared with the less baroclinic atmosphere further south. Over the continental United States, extreme warm summer days tend to be associated with unusually dry surface soil moisture and extreme cool days are often associated with unusually moist soil moisture (especially in the western United States).

Associations between ENSO and extreme temperature days tend to be weak in the findings of this work. There is a slight increase in significant association between ENSO and extreme temperature months. While ENSO can have an impact on local temperature, results suggest that other mechanisms are substantially more important for the occurrence of extremes in both the winter and summer. Because ENSO is defined by SST anomalies in the equatorial Pacific Ocean, if follows that associations would be weaker over North

America than in the cases of the PNA and NAM which are defined by atmospheric circulation anomalies with centers of action over the continent.

Based on this analysis, in many locations extreme temperatures are often associated with a particular phase of either the NAM or PNA; however, synoptic-scale weather patterns are critical to the occurrence of days in the tails of the temperature distribution on the daily timescale. Even in areas that are highly associated with either of the circulation patterns, many days can occur while the most influential pattern is not in the preferred amplified state, or in some cases in the opposite phase of the pattern. On monthly timescales, the influence is stronger and fewer months occur outside of the phase of primary association in areas of strong influence. While summertime extremes are affected less by large-scale circulation than winter extremes, other influential factors (including anomalous soil moisture) may be related to larger-scale patterns of anomalous moisture and temperature. A more comprehensive analysis of mechanisms that affect the surface radiation balance in summer months would help identify other important mechanisms and their causes for summer extremes.

b. Summary of Model Analysis

The results from a systematic evaluation of a suite of seventeen state of the art climate models from the CMIP5 database suggests that the most models generally realize the broad features in atmospheric circulation patterns associated with model simulated extreme temperature days. Substantial variability amongst models within the seventeen-member suite does suggest that some models may be better suited for analysis of future

changes in extremes. Even for models that are relatively realistic in their simulation of the circulation patterns associated with extreme temperature days, some geographic regions are more realistically simulated than others. Regions with complex topography, marine influence, or strong asymmetries between patterns associated with cold and warm extremes tend to be the scenarios associated with the most model error.

Winter patterns are more realistically simulated than summer patterns, in general. This is likely due to the larger scale of circulation patterns that make up winter composite patterns and the lower intra-composite variability in daily patterns in the winter. In the summer, weaker, smaller-scale circulation and regions where there is not a strongly preferred circulation pattern associated with temperature extremes are also simulated less realistically by the models as a whole. In general, patterns at Z500 are more realistically simulated compared with SLP patterns likely because there is more variability in SLP patterns than Z500. When a multi-model ensemble mean is constructed for examining circulation patterns, the results are generally more similar to observations than any individual model.

The results from this analysis suggest that some models may be more realistic in their representation of the important mechanisms associated with extreme temperature days than others. Using this information, future analysis of global warming simulations from the models that tend to simulate these patterns more realistically will help the understanding of the mechanisms associated with changes in future temperature extremes. If circulation patterns associated with end of the 21st century extremes do not change appreciably or systematically from the historical simulations, a general warming and a consequent shift of the temperature probability density function (PDF) toward

higher values would likely be the main cause of changes in extremes. It is also possible that, in some places, the circulation patterns themselves change as a result of anthropogenic global warming. In this scenario, the shape of the temperature PDF could change, potentially affecting the tails and the behavior of extreme events. Information on expected changes in circulation for places where temperature extremes may be sensitive to small changes in circulation (such as locations near influential bodies of water) could also be gained by analysis of future climate model simulations.

5.2. Broader implications

The findings of this work suggest that in most parts of North America, synoptic-scale, transient circulation patterns are the key mechanism associated with extreme temperature days. Because of the importance of these patterns, any systematic change due to anthropogenic climate change in these patterns would affect extreme temperatures over North America. In regions where the PNA and NAM are particularly influential, a systematic change in the phase or strength of these patterns would also result in a subsequent change in the temperature PDF. In some cases, such a change could conceivably have an influence that could counter a decrease in extreme cold events and an increase in extreme warm events that would be expected from an overall global warming. These nonlinear changes in the temperature PDF could result in regions that experience distinctive changes as a result of global warming that differ considerably from the majority of the globe.

In order for climate models to realistically simulate the severity, frequency, and duration of extreme temperature events in global warming scenarios, they need to realize the scale and strength of these important patterns in historical simulations. In general, the majority of the models analyzed here capture the correct scale and strength of these patterns in most places at most times of the year. It is particularly important, yet seemingly difficult, for the models to capture the correct circulation patterns in areas that may be particularly sensitive to small changes in circulation (such as the Alaska example in Chapters 2 and 4). These areas are often affected by complex topography or large water bodies that are difficult to capture with a gridded dataset and may cause challenges in model simulations. Because changes in circulation in these regions will likely result in non-linear shifts in the temperature PDF, understanding of the uncertainty in model simulation of these regions is key to being able to anticipate future changes in regional temperature extremes. Furthermore, although not explicitly investigated in this work, a correct representation of larger-scale circulation (i.e. PNA and NAM) is also important for models to capture as these patterns are important mechanisms in many parts of the continent.

5.3. Limitations and Future Direction

The analysis of historical simulations from a suite of climate models performed here will allow for better interpretation of projected changes in simulations of future climate. Each model analyzed in this work has also simulated future climate under two emissions scenarios (RCP4.5 (lower) and RCP8.5 (higher)). Changes in the circulation patterns in future global warming scenarios would provide information on the mechanisms for

changes in extremes. This will also allow for quantification of uncertainty in future projections of extreme temperatures in each model. In addition to changes in circulation, changes in the temperature PDF for each grid cell would further shed light on the mechanisms responsible for the changes projected by each model. This analysis will test the hypothesis that changes in extremes are only a result of a shift to the right of the temperature PDF at all location and not because of changes in circulation affecting the shape of the PDF. This could also test how sensitive different regions are to slight shifts in circulation and if these shifts are projected in global warming simulations.

There are other influential physical processes that were not examined in this work that are important for models to realistically capture for a comprehensive analysis of future simulations. Soil moisture, for example, is an important variable for summertime extreme temperature events. An analysis of the relationship between model simulated soil moisture and extreme temperatures would add another important piece of information towards a comprehensive understanding of the level to which models represent the mechanisms associated with extreme temperatures.

This project utilized temperature observations and global reanalysis data on a relatively coarse grid. The main benefit to using this temperature anomaly product is that the dataset is based on surface temperature observations, which are not used in global reanalysis products. The global reanalysis was chosen because large-scale circulation patterns, especially the recurrent modes of variability that were investigated, are often too large to be fully captured by a regional reanalysis product. In many cases; however, the resolution of the data used here is too low to capture extreme events that may occur on smaller scales or due to smaller-scale processes that may also be important mechanisms.

This is likely a more substantial limitation near coastlines and in mountainous regions where slight variations in location may be associated with large changes in weather and climate. The use of higher resolution products such as regional reanalysis and models could help answer questions about the processes associated with extremes that occur in regions with high spatial variability in climate due to complex terrain or proximity to large bodies of water.

One location where this limitation is particularly acute is the Pacific Coast of the southwestern United States. Here a combination of mountains and marine influences combine to cause a sharp skewness gradient (Figure 5.1). Here, areas closer to the coast exhibit long warm tails as indicated by the positive skewness values while areas a short distance inland are characterized by temperature PDFs that are weakly or negatively skewed. The North American Regional Reanalysis product used in Figure 5.1 is able to resolve these changes in the shape of the temperature PDFs in this region, but the coarser grid of the HadGHCND data set (Figure 2.5) is unable to show this feature in detail as a single grid cell encompasses the coastal, mountainous, and desert climates of this region. The atmospheric circulation pattern that favors extreme events along the coast is likely different from that associated with extreme events further inland, but this pattern cannot be captured using coarser resolution data. Using regional data to more closely investigate extreme events and the mechanisms associated with them could lead to a more comprehensive understanding of the physical mechanisms as well as how extremes in these locations may change in the future.

Model Name	Horizontal Resolution (lat x lon)	Modeling Group	Z500 Available
BNU-ESM	2.81x2.81	GCESS, China	Yes
CanESM2	2.81x2.81	CCCma, Canada	Yes
CMCC-CM	0.75x0.75	CMCC, Italy	Yes
CNRM-CM5	1.41x1.41	CNRM-CERFACS, France	Yes
FGOALS-g2	3.00x2.81	LASG-CESS, China	Yes
FGOALS-s2	1.67x2.81	LASG-IAP, China	Yes
GFDL-ESM2G	2.00x2.50	GFDL, United States	No
GFDL-ESM2M	2.00x2.50	GFDL, United States	Yes
HadGEM2-CC	1.25x1.88	MOHC, United Kingdom	Yes
INM-CM4	1.50x2.00	INM, Russia	No
IPSL-CM5A-LR	1.88x3.75	IPSL, France	Yes
IPSL-CM5A-MR	1.26x2.50	IPSL, France	Yes
MIROC5	1.41x1.41	MIROC, Japan	Yes
MIROC-ESM-CHEM	2.81x2.81	MIROC, Japan	Yes
MPI-ESM-LR	1.88x1.88	MPI-M, Germany	Yes
MPI-ESM-MR	1.88x1.88	MPI-M, Germany	Yes
MRI-CGCM	1.13x1.13	MRI, Japan	Yes

Table 4.1. List of the 17 CMIP5 models used.

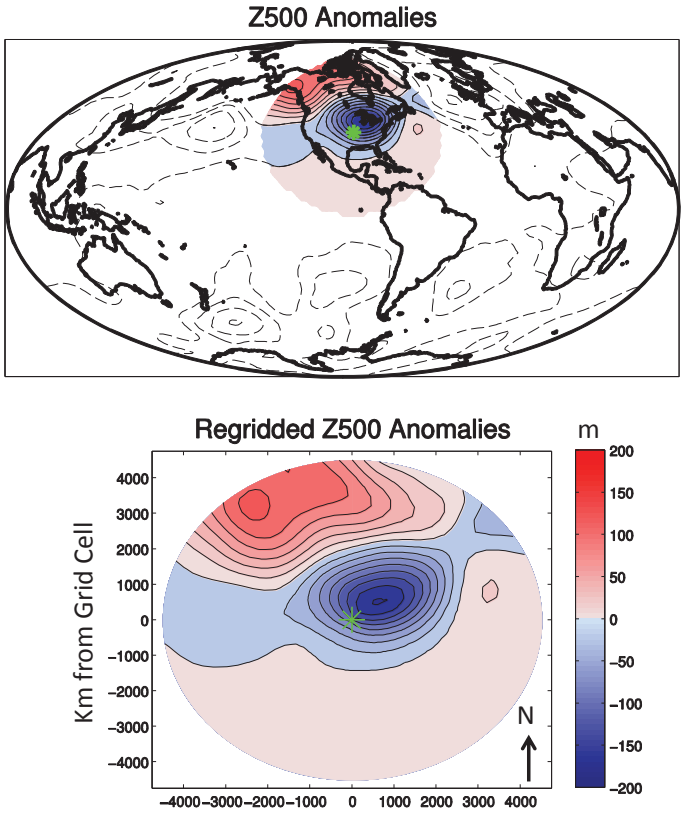

Figure 2.1. An illustration of how the grid-cell relative composites were created. The top plot is a map of Z500 anomalies associated with January extreme cold days at the grid cell represented by the green star. Only data within 4500 km of the grid cell is shaded. That map was then interpolated onto the grid-cell relative grid in the bottom plot such that the center of the circle is the grid cell where the extreme temperatures are being computed. This was done for all grid cells over North America for all composites.

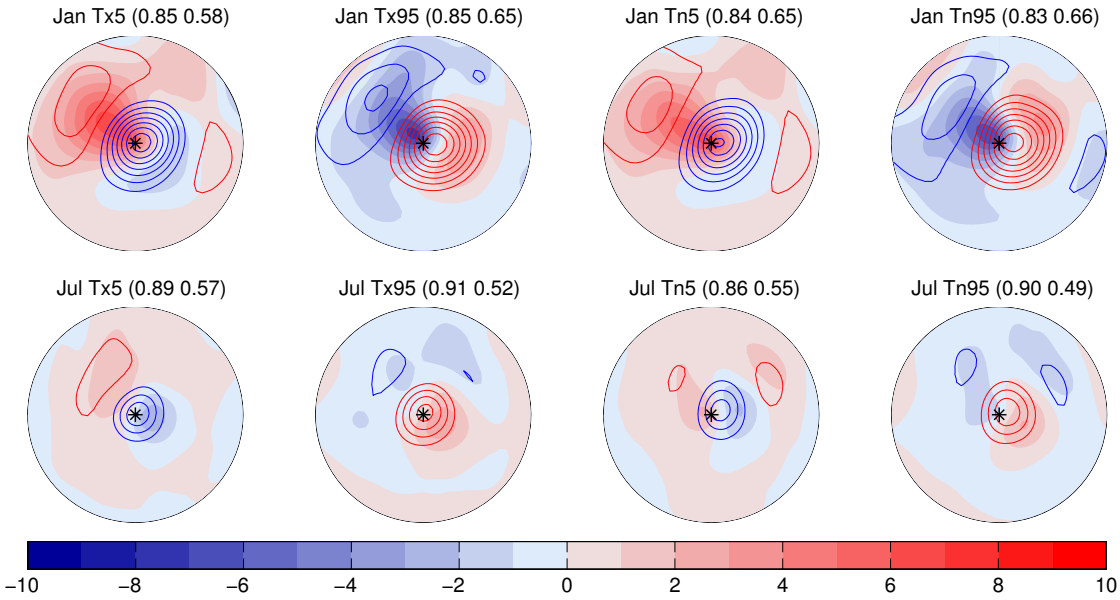

Figure 2.2. Grand composites of anomalies for all 315 grid cells. SLP anomalies in hPa are shaded and Z500 height anomalies are contoured every 20 meters. Red contours are positive Z500 anomalies and blue contours are negative. The top column shows grand composites for January and bottom for July extreme (from left to right) cold maximum (Tx5), warm maximum (Tx95), cold minimum (Tn5), and warm minimum (Tn95) temperatures. The values to the right of the titles represent the median pattern correlation coefficient when the grand composite for Z500 (left value) and SLP (right value) is correlated with all individual composites for the entire continent.

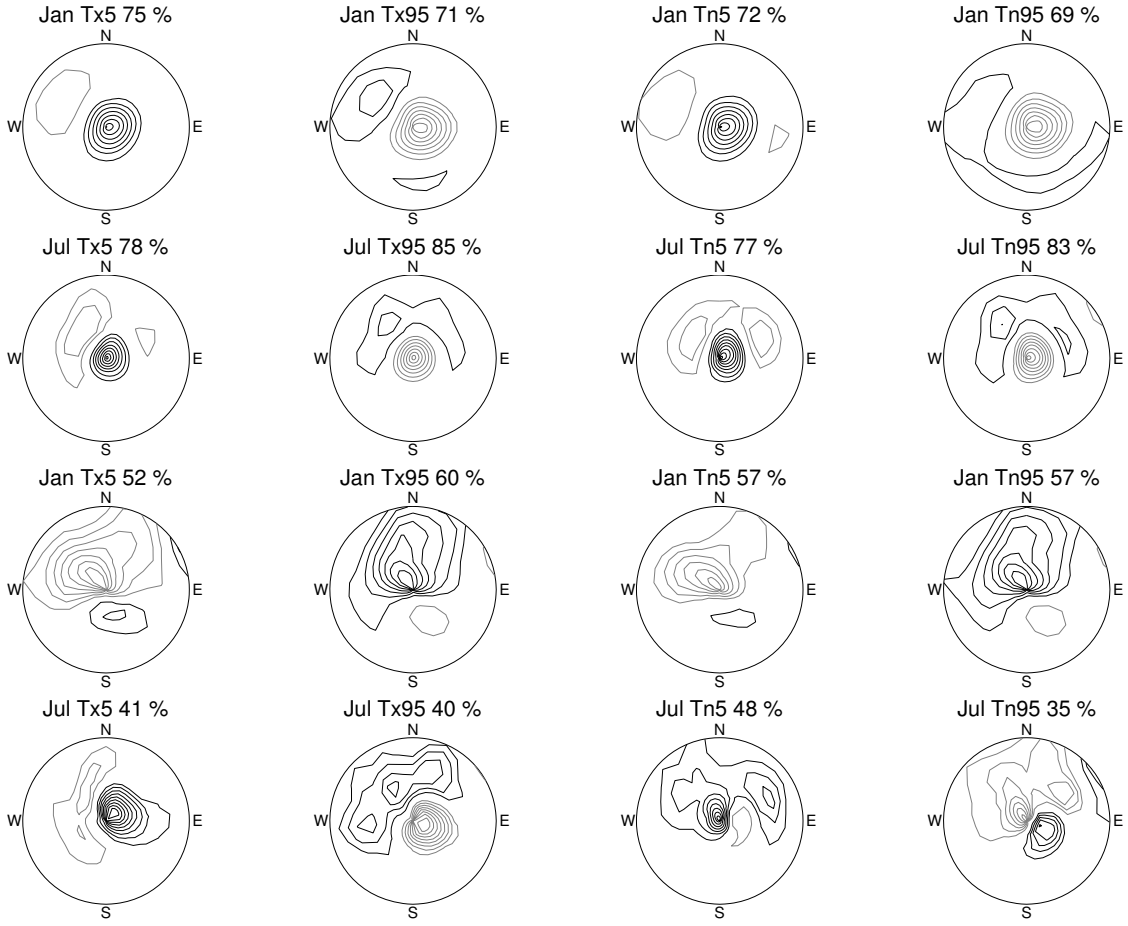

Figure 2.3. The leading EOF of Z500 (top 8) and SLP (bottom 8) obtained when EOF analysis is performed on the 315 different composites for each grid cell in North America. Black contours are positive values and gray contours are negative. The variance explained by each first EOF is plotted with the title. The types of extremes match those of figure 2.

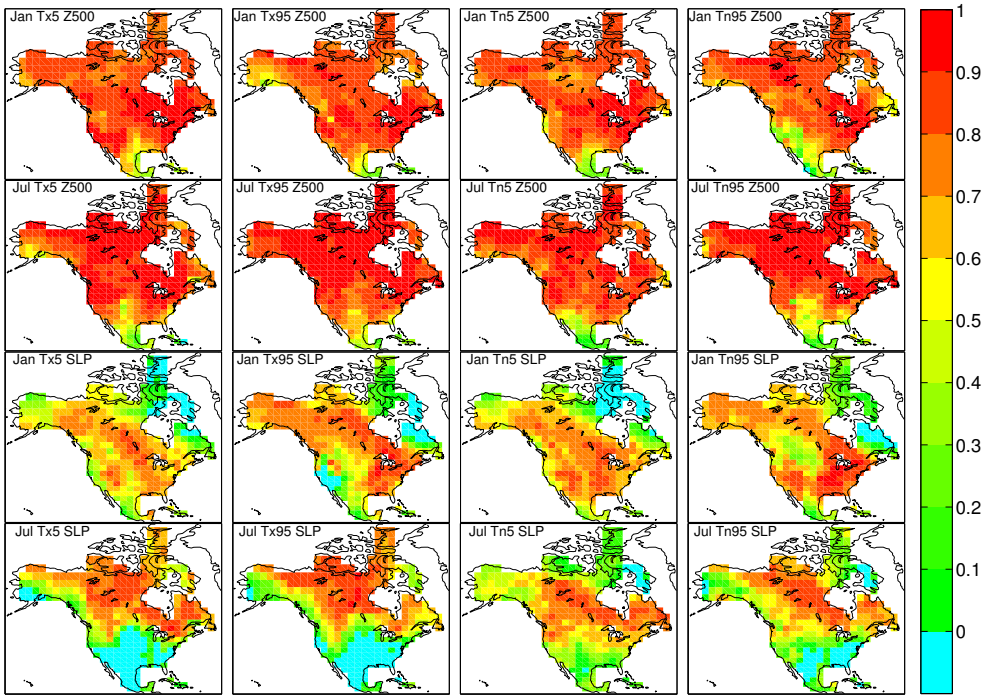

Figure 2.4. Coefficients from a pattern correlation between the composite pattern at each grid cell and the corresponding grand composite in Figure 2. Higher values indicate places where the local pattern resembles the grand composite for the indicated extreme. Areas where the correlation is less than 0 are shaded in blue but not contoured.

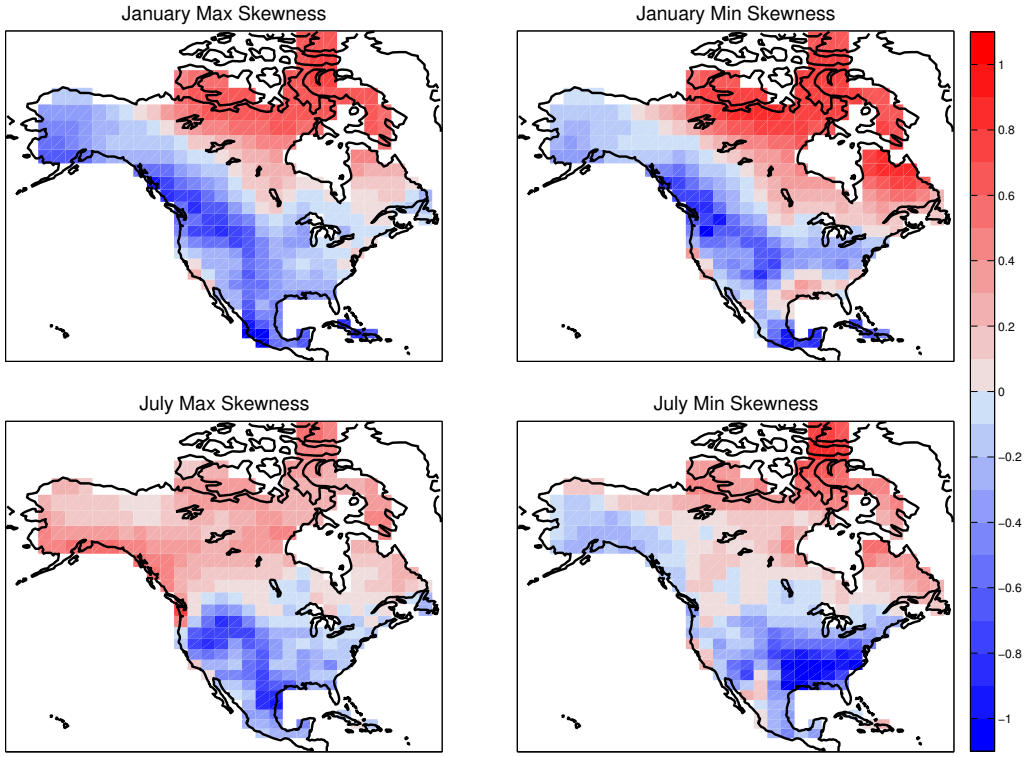

Figure 2.5. Plots of skewness for January and July maximum and minimum temperature anomalies for all 30 years of data.

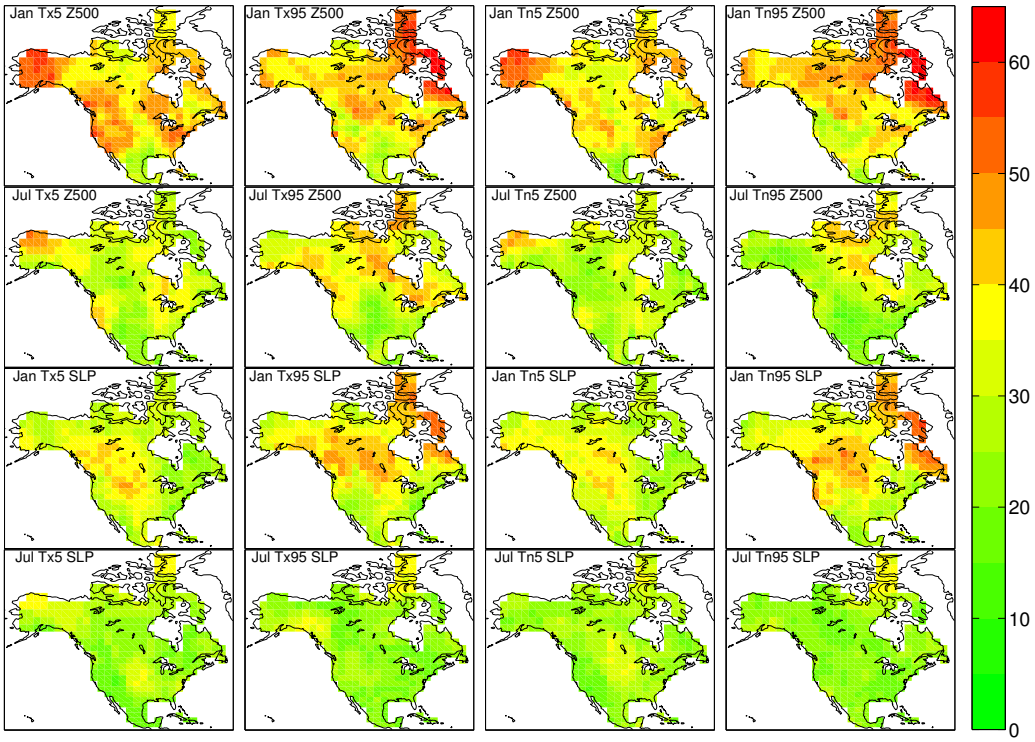

Figure 2.6. Variance explained, in percent, by the leading EOF of the daily patterns comprising the composite for each grid cell for the indicated extreme. Areas with higher variance explained have less variability within the composites.

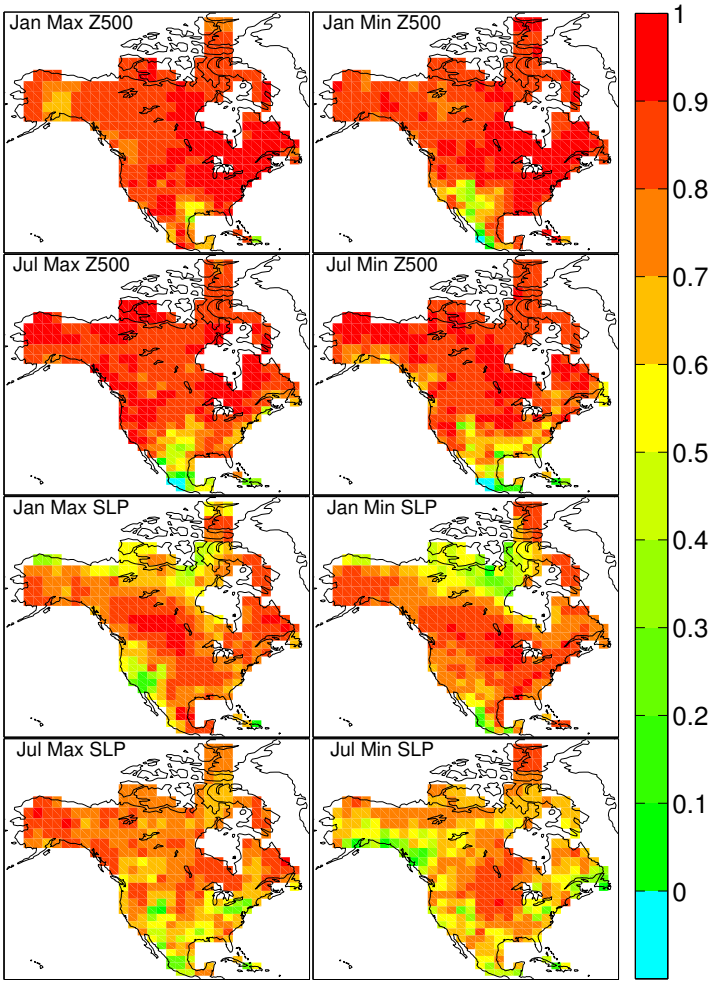

Figure 2.7. Maps of symmetry computed by calculating the coefficients from a pattern correlation between the composite pattern for extreme warm days and extreme cold days. Each coefficient was multiplied by -1 so that a higher positive correlation equates to areas with more symmetrical pattern pairs. The top four panels are for Z500 and the bottom four are for SLP anomaly patterns. Plots labeled “Min” are the correlation between the extreme cold minimum and the extreme warm minimum and the plots labeled “Max” are the same but for the extremes in maximum temperatures.

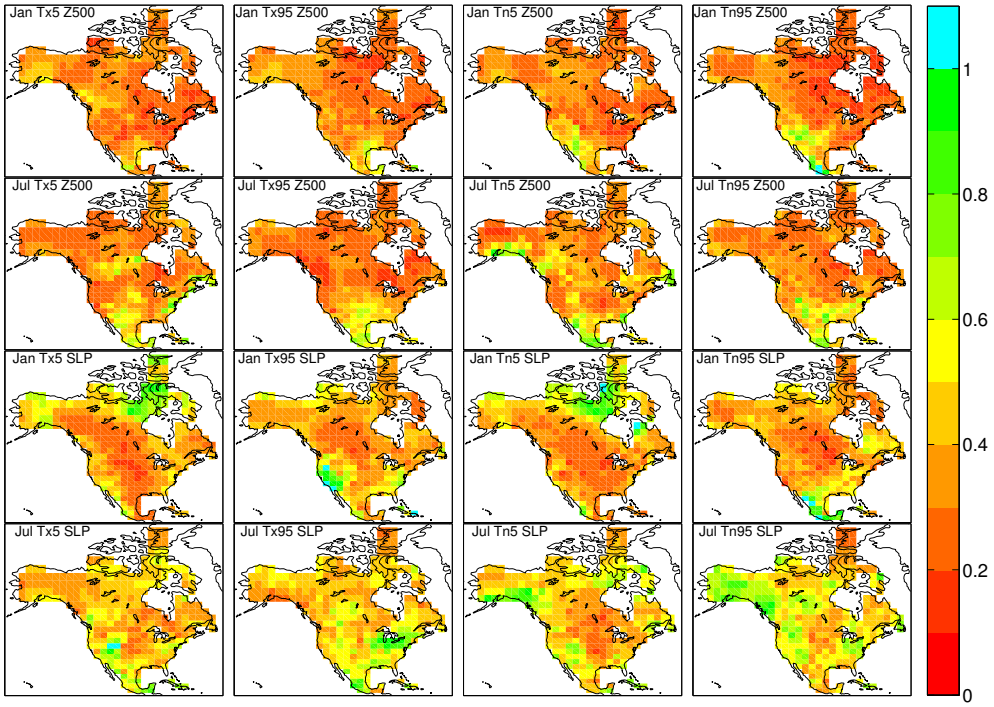

Figure 2.8. Maps of linearity, calculated by computing the RMS error between the composite pattern for each grid cell and the linear regression pattern for each grid cell. The regression pattern is computed by regressing the entire time series of Z500 anomalies (top 2 rows) and SLP (bottom 2 rows) for each grid cell on the entire time series of temperature anomalies at the grid cell where the extreme temperatures are occurring. The regression coefficients are multiplied by the mean temperature anomaly in the specific tail so that both composite patterns and regression patterns have the same units. The RMS error is normalized by the standard deviation of the composite pattern. Higher values indicate where the patterns are less linear and lower values are where patterns are more linear.

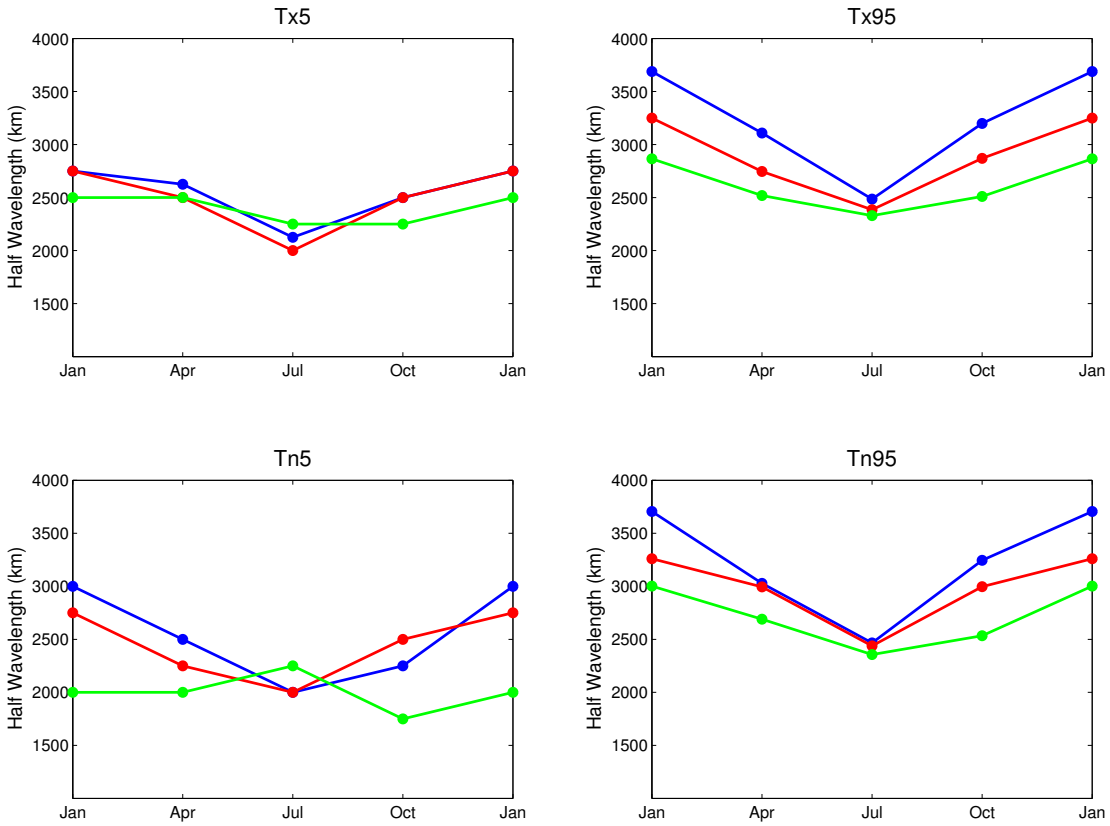

Figure 2.9. The median half-wavelengths for three latitude bands for the entire seasonal cycle as represented by the four months analyzed. Each half-wavelength is the distance in kilometers (y-axis) between the largest positive and negative normalized anomalies in Z500. The median is computed from the half-wavelength values for every grid cell north of 57.5 (blue), between 37.5 and 57.5degrees (red), and south of 37.5 (green) degrees north latitude.

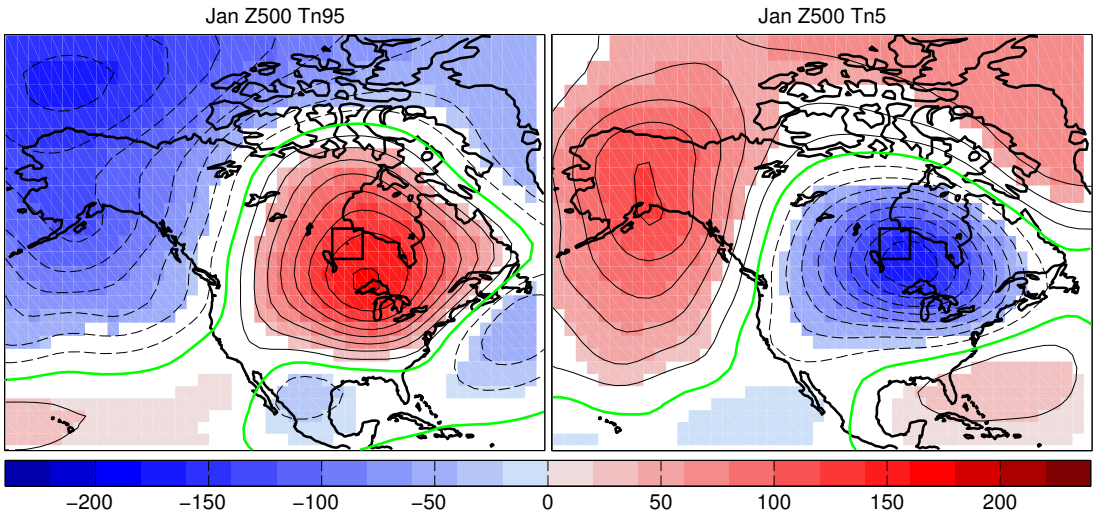

Figure 2.10. Composite patterns of the anomalies in Z500 (contoured every 20 meters) in the area highlighted by the black box concurrent with extreme warm (left) and extreme cold (right) daily minimum temperatures in January. The thick green line is the zero meter contour. Only values that are statistically significant at the five percent level are shaded.

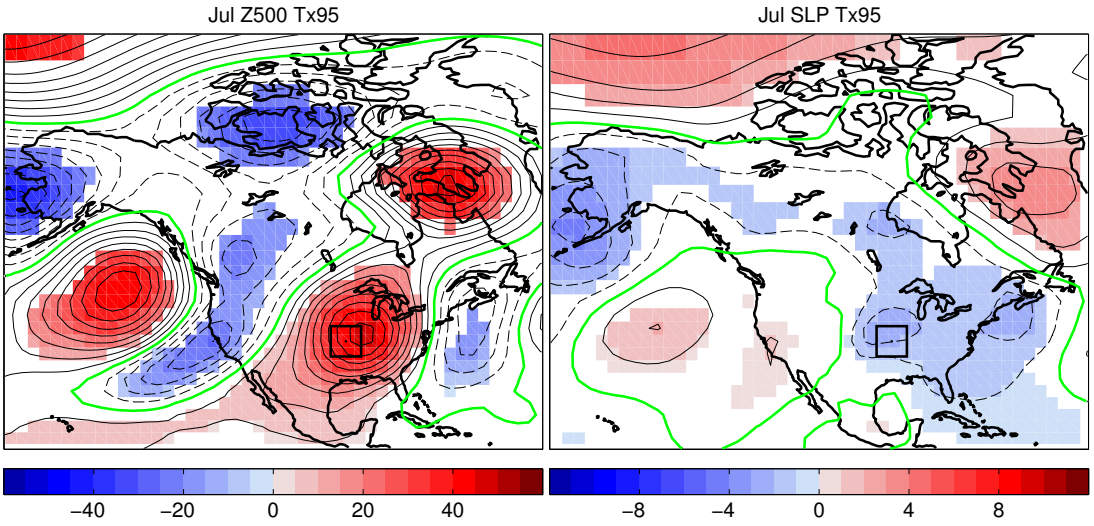

Figure 2.11. Composite patterns of the anomalies in Z500 (left, every 5 meters) and SLP (right, every 1 hPa) in the area highlighted by the black box for extreme warm daily maximum temperatures in July. The thick green line is the zero meter/hPa contour. Only values that are statistically significant at the five percent level are shaded.

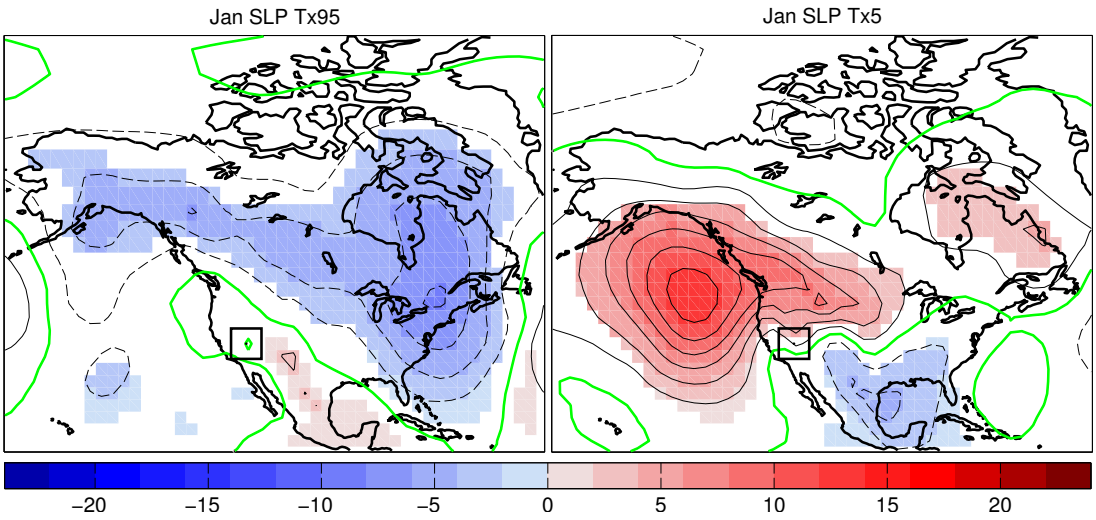

Figure 2.12. Composite patterns of the anomalies in SLP (contoured every 2 hPa) in the area highlighted by the black square concurrent with extreme warm (left) and extreme cold (right) daily maximum temperatures in January. The thick green line is the 0 hPa contour. Only values that are statistically significant at the five percent level are shaded.

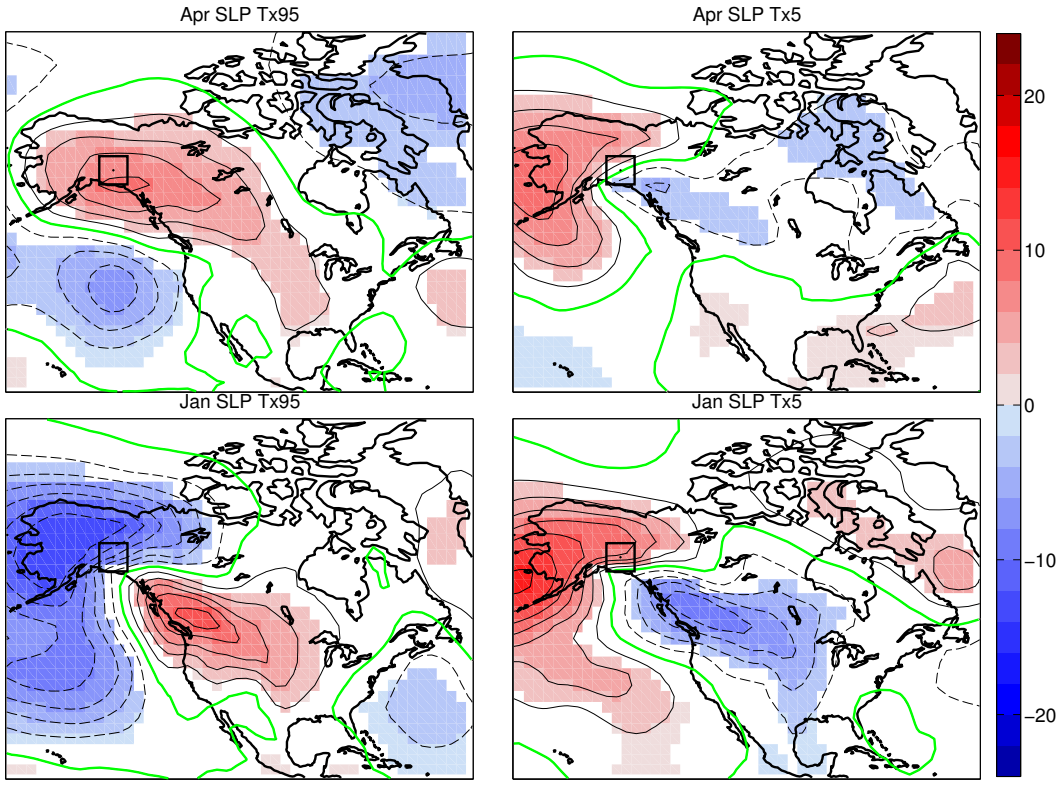

Figure 2.13. Composite patterns of the anomalies in SLP (contoured every 2 hPa) in the area highlighted in green concurrent with extreme warm (left) and extreme cold (right) daily maximum temperatures in April (top) and January (bottom). The thick green lines is the 0 hPa contour. Only values that are statistically significant at the five percent level are shaded.

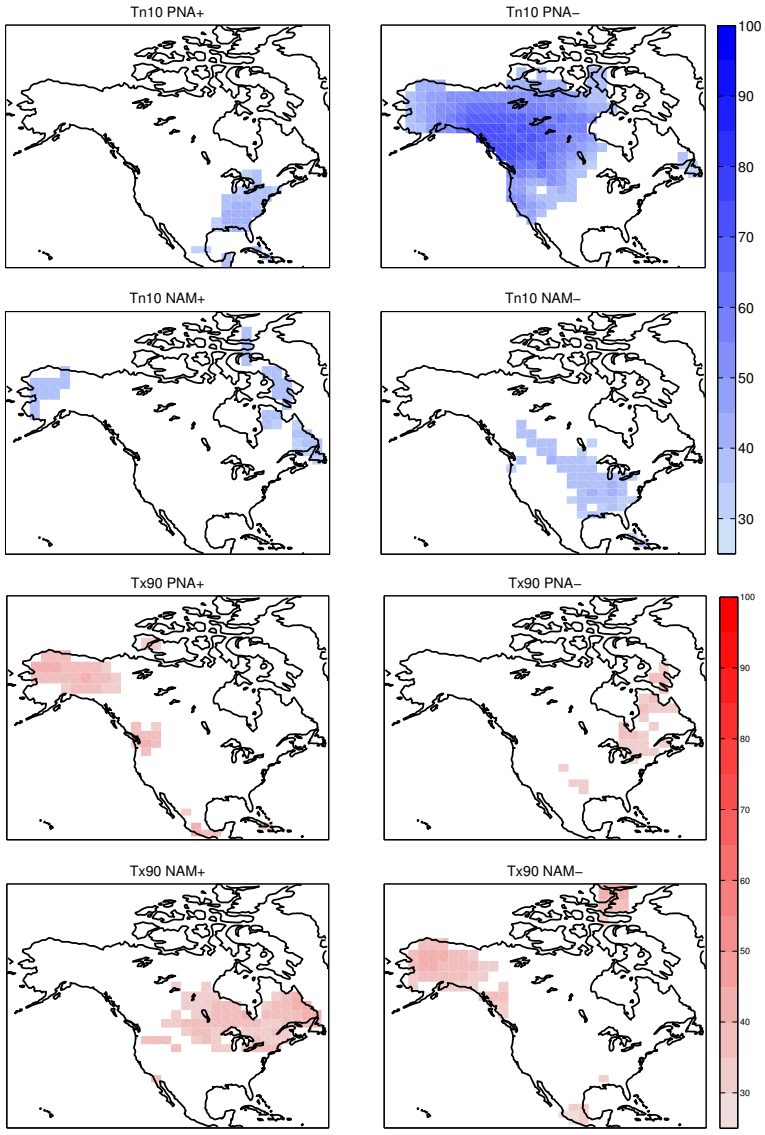

Figure 3.1. The percentage of extreme cold DJF minimum temperature days (a) and extreme warm JJA maximum temperature days (b) that occur when the PNA or NAM are in the upper (+) or lower (-) quartile of the index value distribution. Only grid cells where the percentage is significantly greater than expected by chance at the 5% level are shaded.

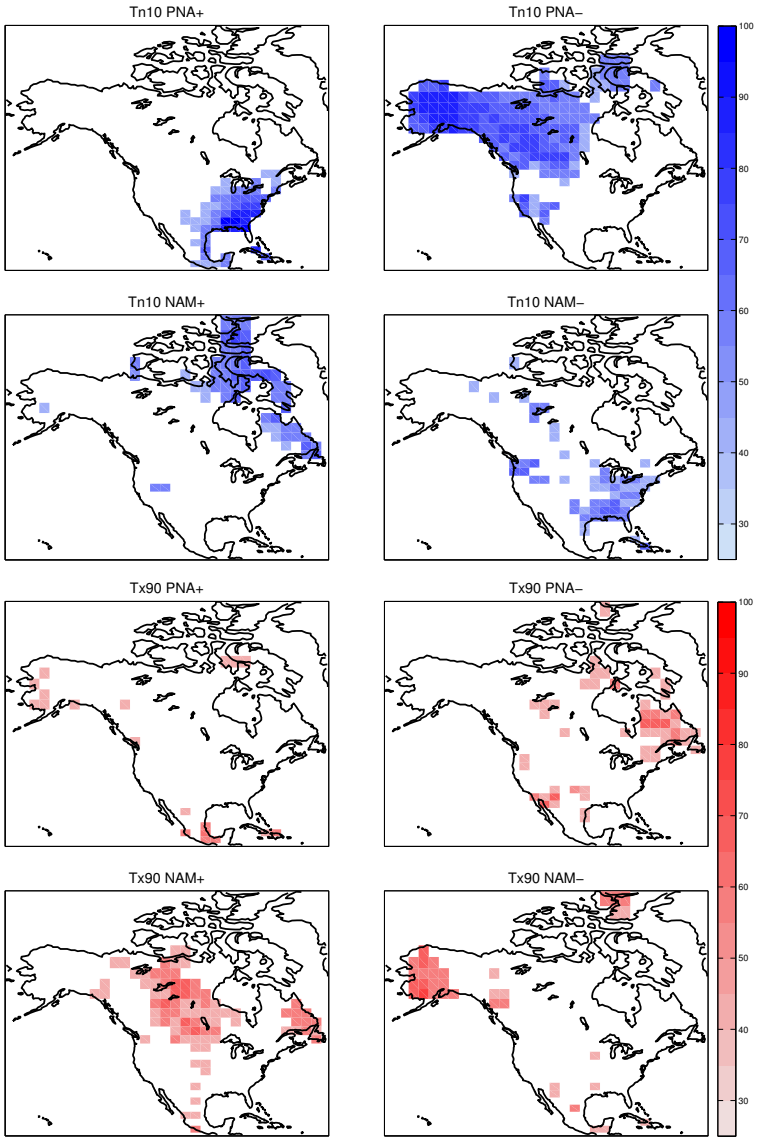

Figure 3.2 Same as Figure 3.1, except for monthly mean temperature.

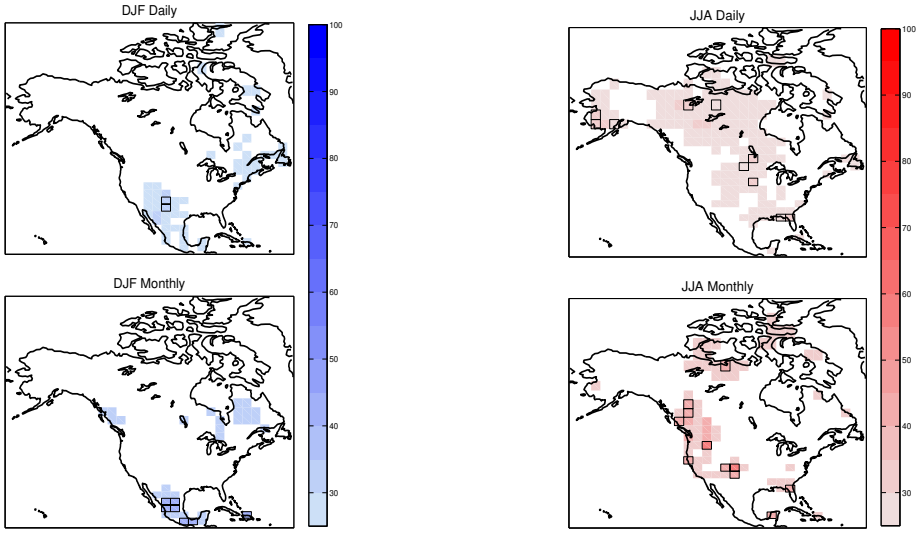

Figure 3.3. The percentage of extreme cold DJF minimum temperature days (top) and months (second from top) and extreme warm JJA maximum temperature days (second from bottom) and months (bottom) that occur when neither the PNA nor the NAM is in the upper or lower quartile. Only grid cells where the percentage is significantly greater than expected by chance at the 5% level are shaded.

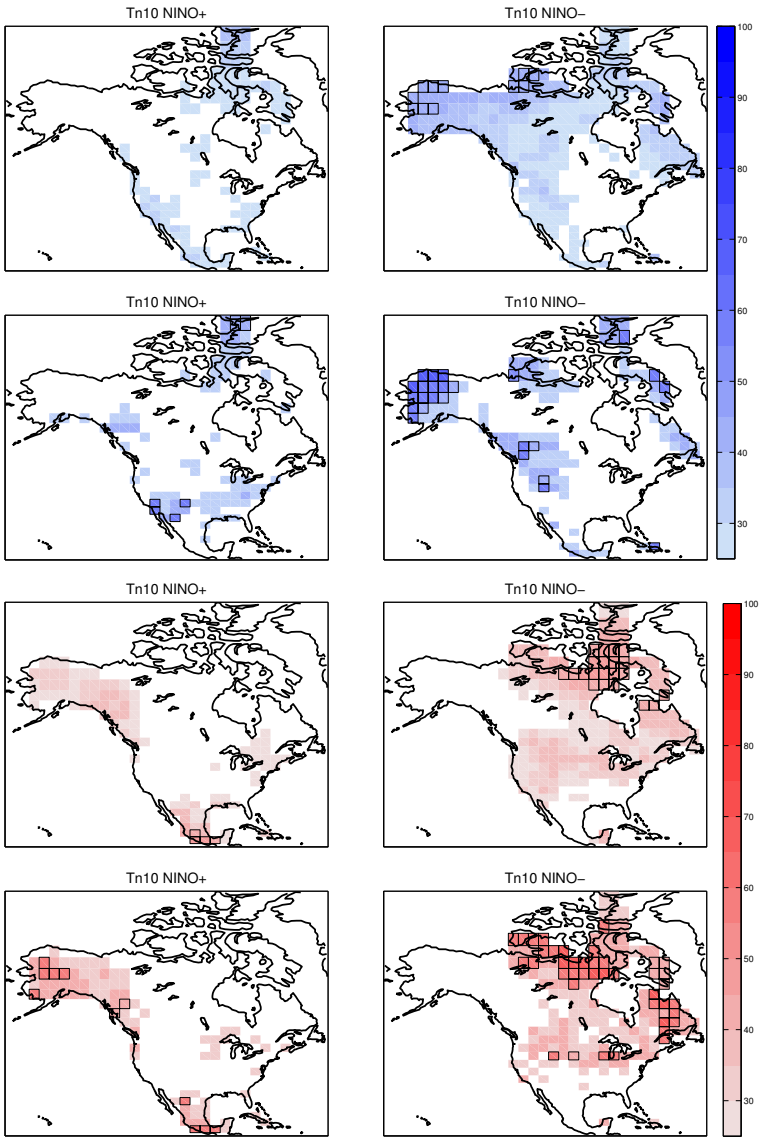

Figure 3.4. The percentage of extreme cold DJF minimum temperature days (top) and months (second from top) and extreme warm JJA maximum temperature days (second from bottom) and months (bottom) that occur when the Niño 3.4 index is in the upper or lower quartile. All grid cells where the percentage is greater than expected by change are shaded and grid cells where the percentage is significantly greater than expected by chance at the 5% level are highlighted.

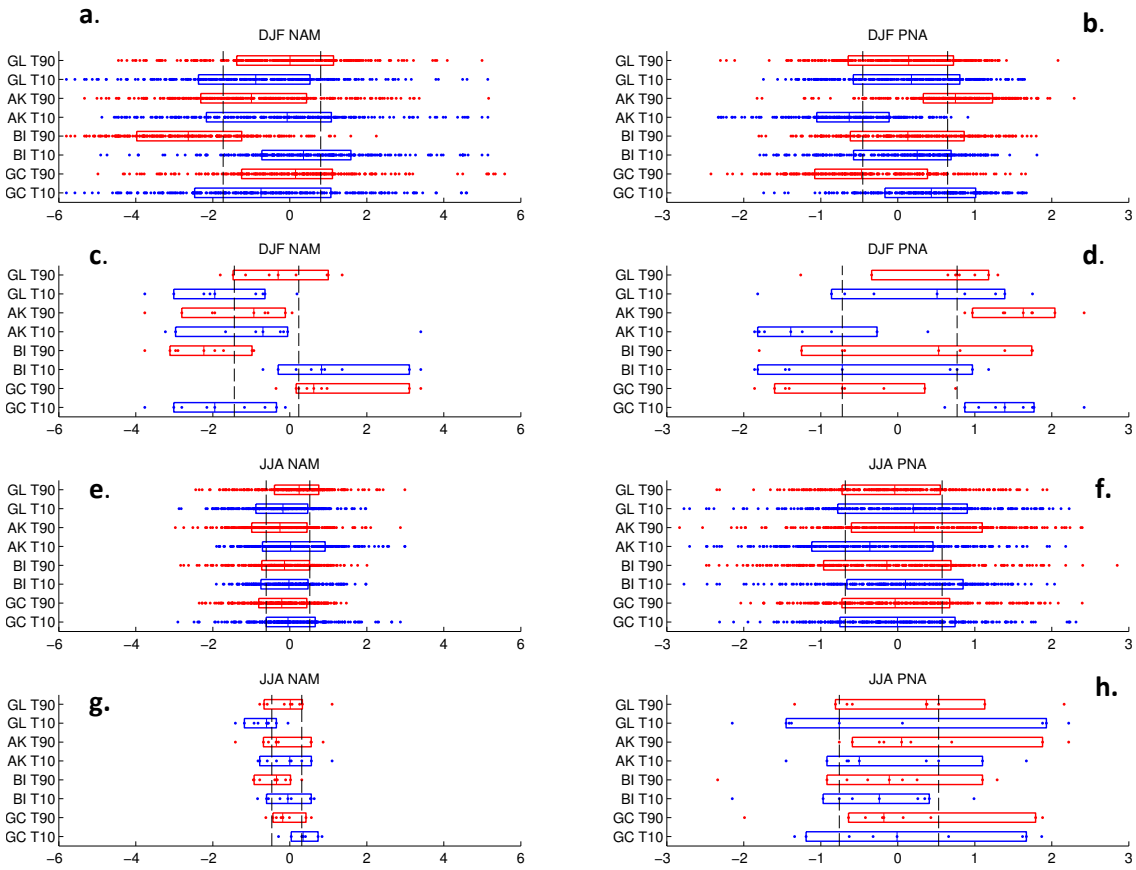

Figure 3.5. Box-and-whisker plots showing the NAM and PNA index values concurrent with cold (blue) and warm (red) extreme minimum DJF temperature days (a, b) and months (c, d) and extreme maximum JJA temperature days (e, f) and months (g, h). Each dot represents one extreme temperature day/month. The box outlines the 25th and the 75th percentiles of index values for that location while the vertical line in the box marks the median. The left column is for the NAM and the right for the PNA. The black vertical lines delineate the lower and upper quartiles of the index values for all days or months for reference with Figure 3.1.

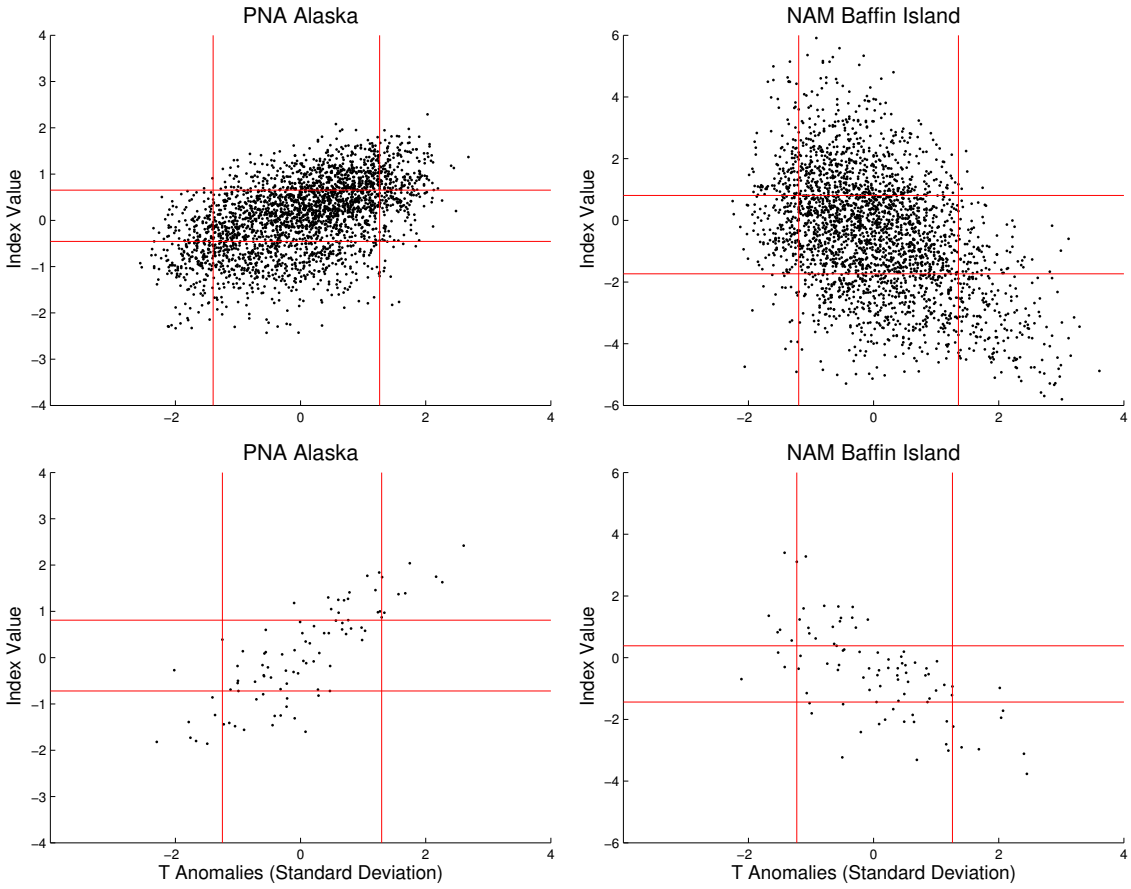

Figure 3.6. Scatter plots of normalized minimum DJF temperature anomalies vs. index values of the PNA for Alaska (left) and the NAM for Baffin Island (right) for daily (top) and monthly (bottom) maximum temperatures.

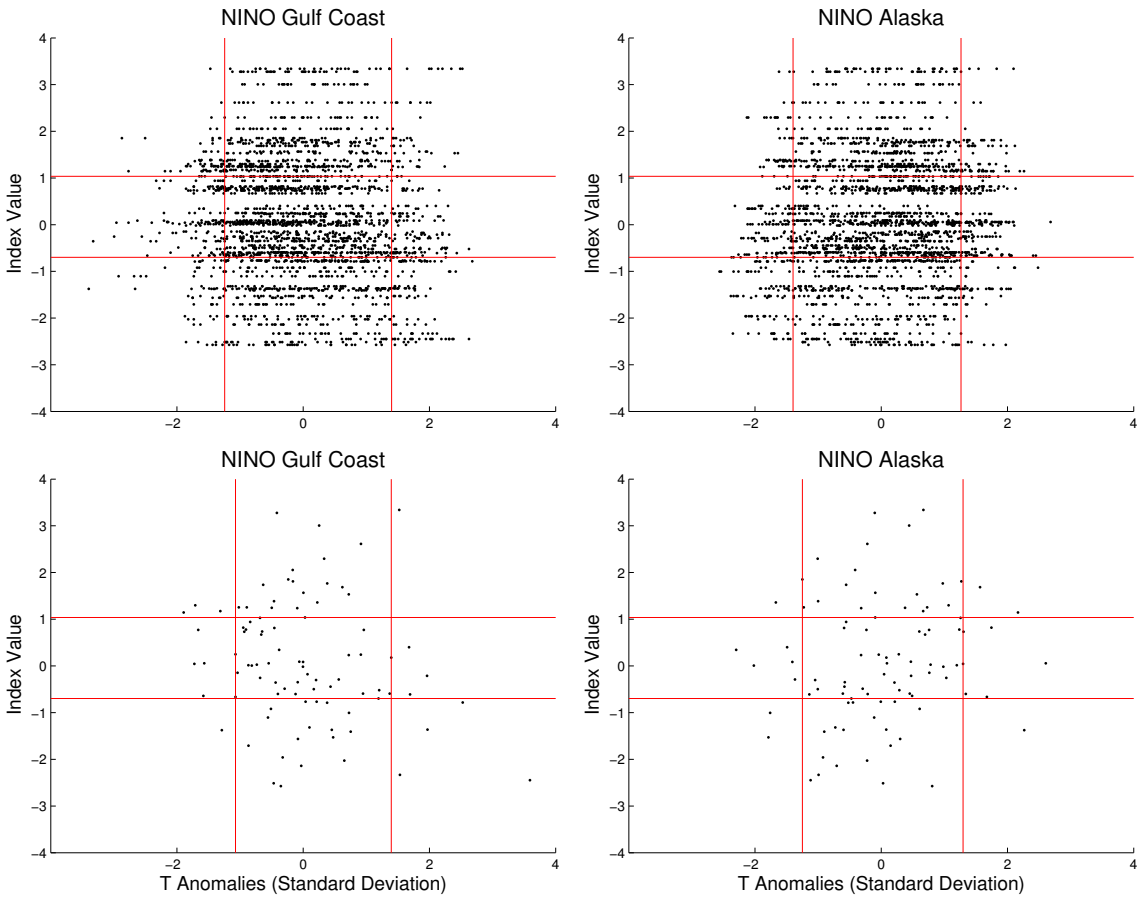

Figure 3.7. Same as Figure 3.6 except for Niño 3.4 at the Gulf Coast left and Alaska right locations.

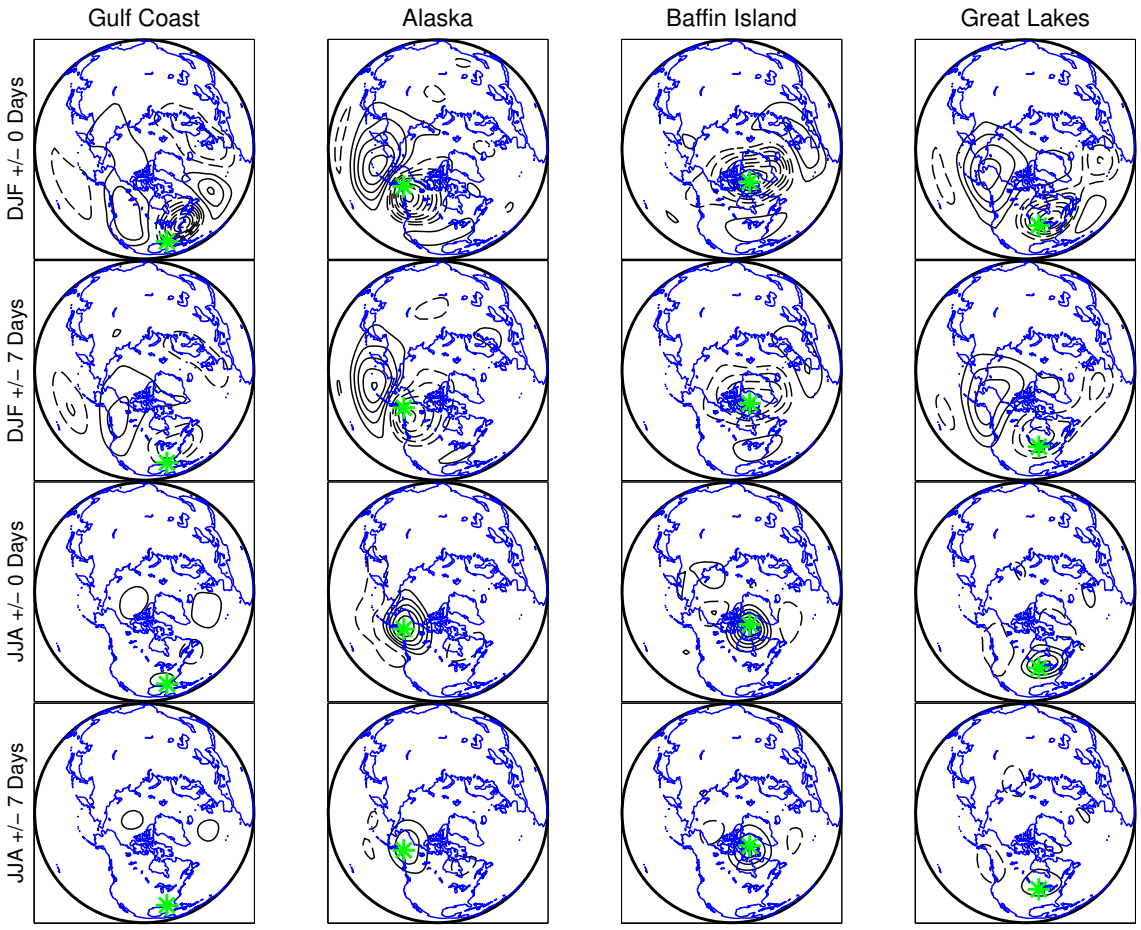

Figure 3.8. Composites of Z500 anomalies for all extreme cold DJF minimum temperature days and all extreme warm JJA maximum temperature days for each of the four locations which are centered on the green star. Negative anomalies are contoured with dashed lines and positive anomalies by solid lines. The contour interval is 20 meters and the zero contour is omitted. Rows labeled with "+/- 0 days" are composites of anomalies for only the extreme temperature days while rows labeled with "+/- 7 days" are composites of the 15-day mean anomaly centered on the extreme temperature day.

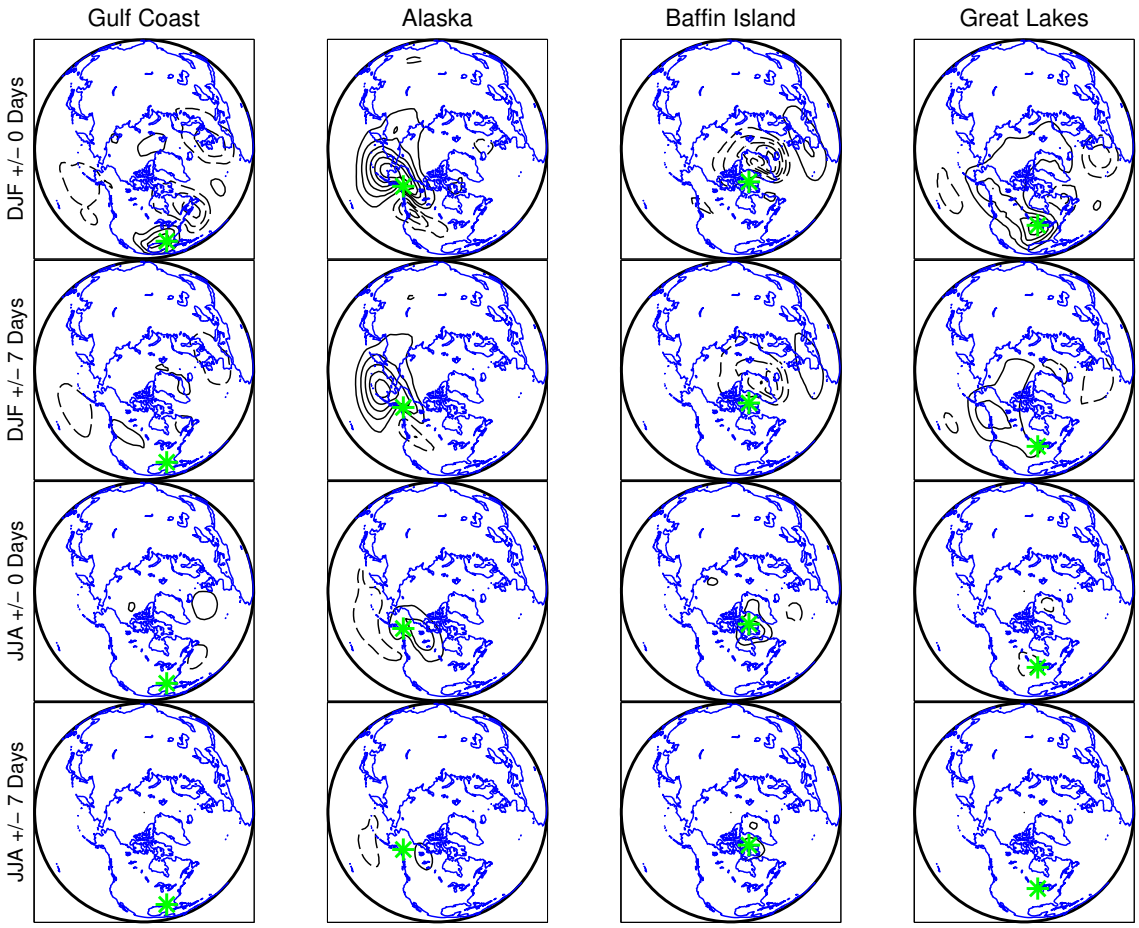

Figure 3.9. Same as Figure 3.7 except for SLP anomalies. Contours are every 2 hPa with the zero contour omitted.

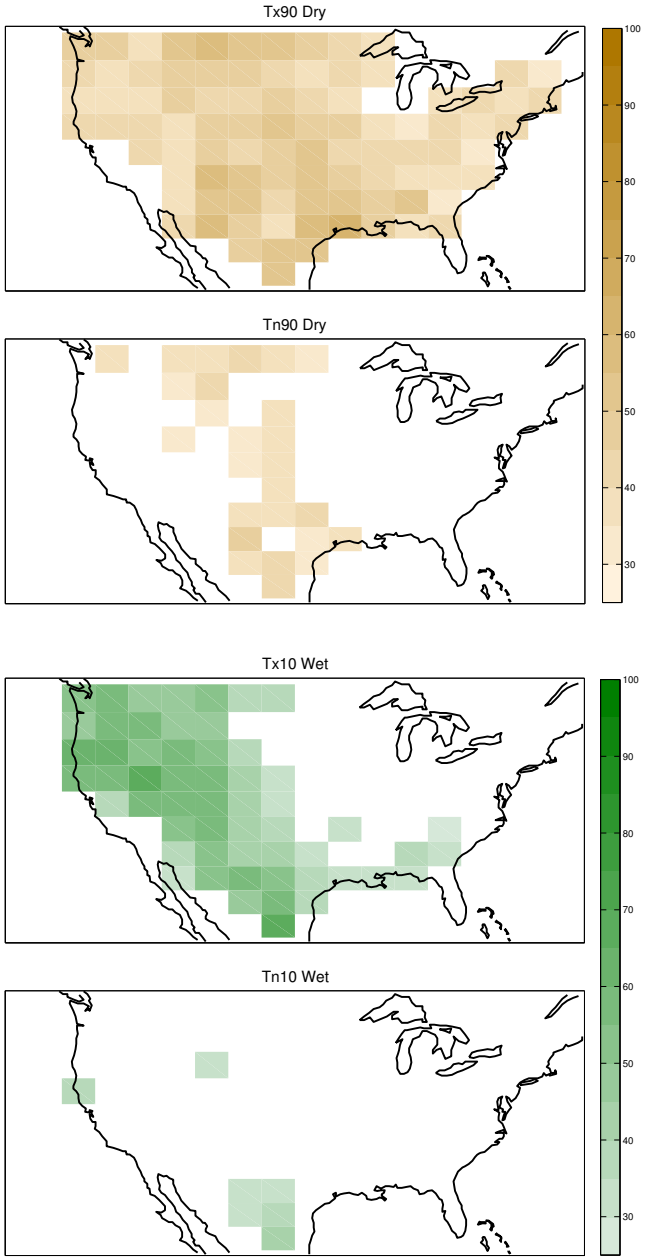

Figure 3.10. The percentage of extremely warm JJA maximum temperature days that occurred when soil moisture was in the driest quartile of days at each grid cell (top 2) and minimum temperature days that occurred when the soil moisture was in the wettest quartile of days at each grid cell (bottom 2).

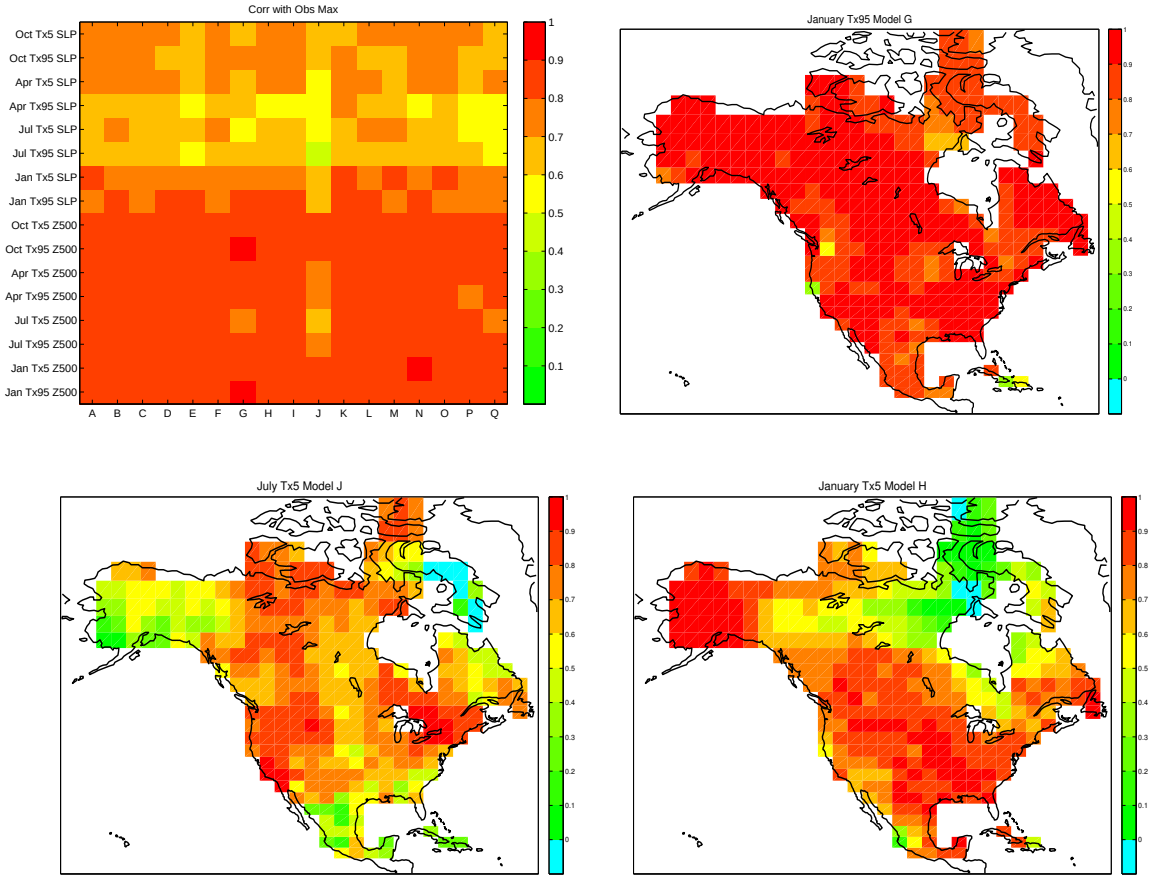

Figure 4.1. (From top left to bottom right) Portrait diagram depicting the median values of the set of pattern correlations between the observed composite pattern at each grid cell and the corresponding simulated composite pattern for each model. Maps of correlation coefficients for select models and extremes: January Tx95 Z500 for model G, July Tx5 Z500 for model J, and January Tx5 SLP for model H.

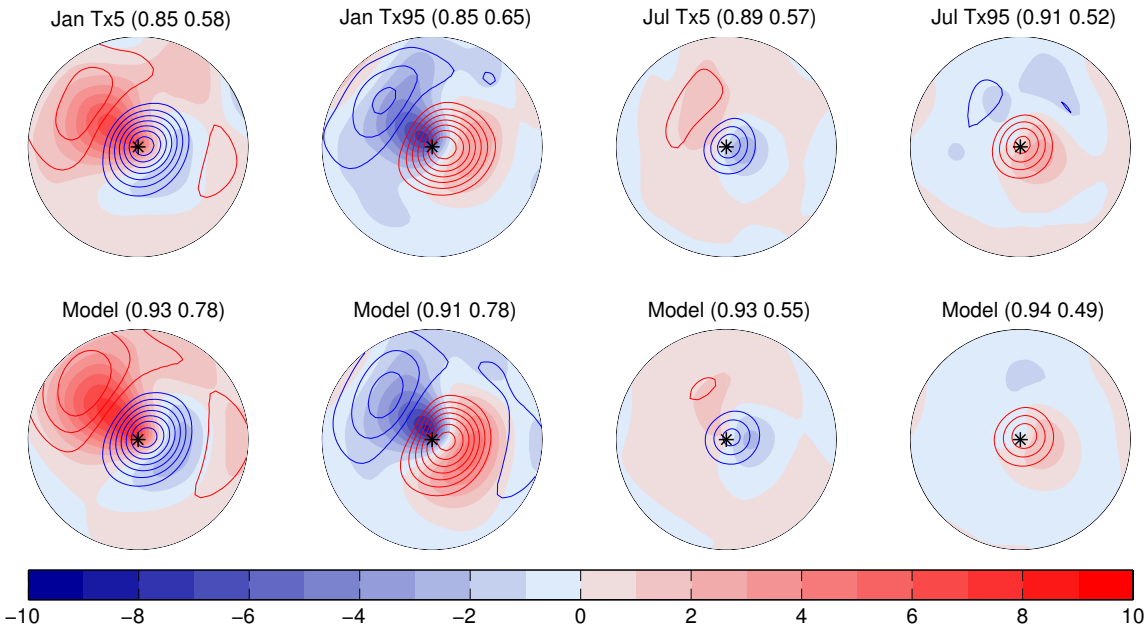

Figure 4.2. Grand composites for (left to right, top) observed extreme cold January, extreme warm January, extreme cold July, and extreme warm July maximum temperature days. The bottom row contains the corresponding grand composites for the multi-model ensemble mean. In both rows, the values next to the title are the median pattern correlation coefficients when individual composite patterns for each grid cell (315 total) over North America are correlated with the grand composite. The left number is for Z500 composites and the right for SLP composites.

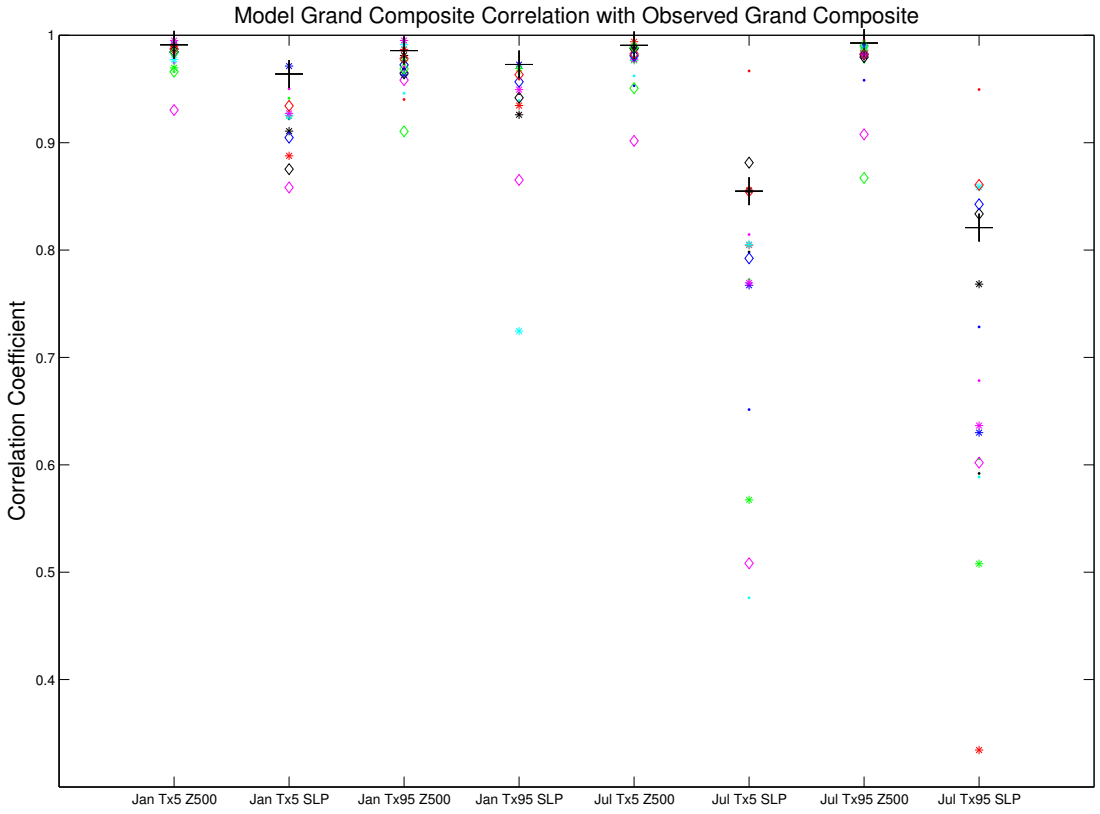

Figure 4.3. Coefficients from a pattern correlation between the grand composite for each model and the observed grand composite. Each symbol is for a different one of the seventeen models and the symbols are consistent among all types of extreme plotted. The multi-model ensemble grand composite correlation coefficient is plotted with a large black cross for each type of extreme.

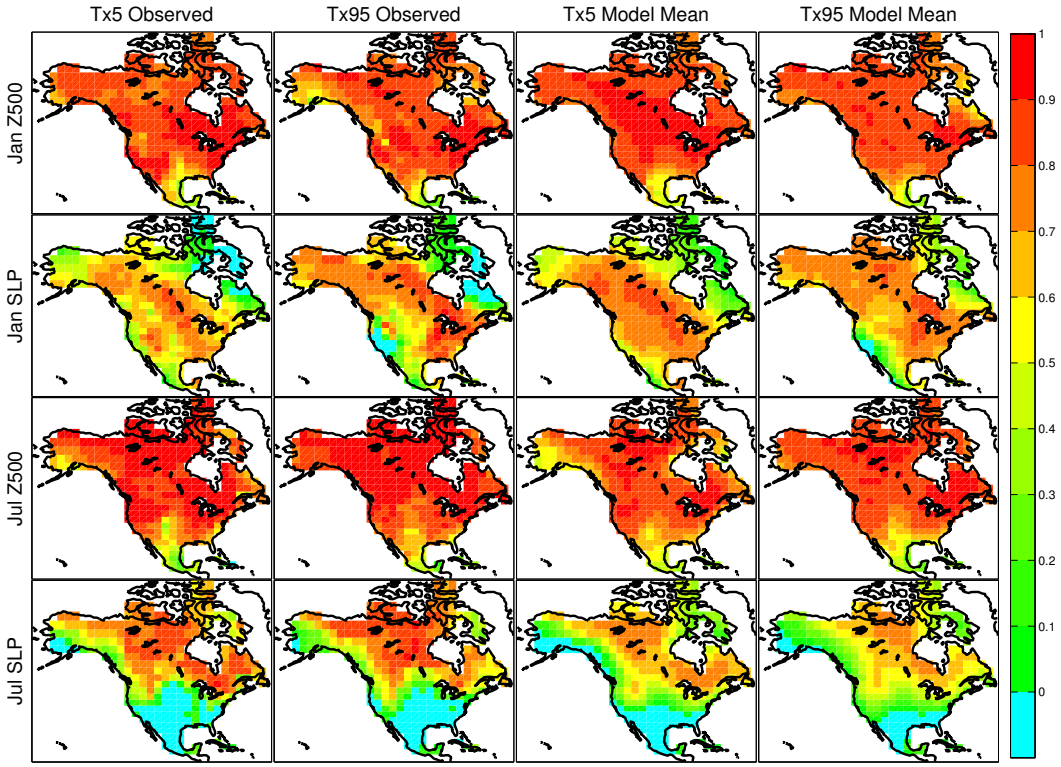

Figure 4.4. Correlation coefficients when the composite pattern for each grid cell is correlated with the grand composite. The left two columns are for the observed patterns and the right two columns are the average pattern correlations from all seventeen models. All extremes are for daily maximum temperatures and the top two rows are for January and the bottom two rows for July.

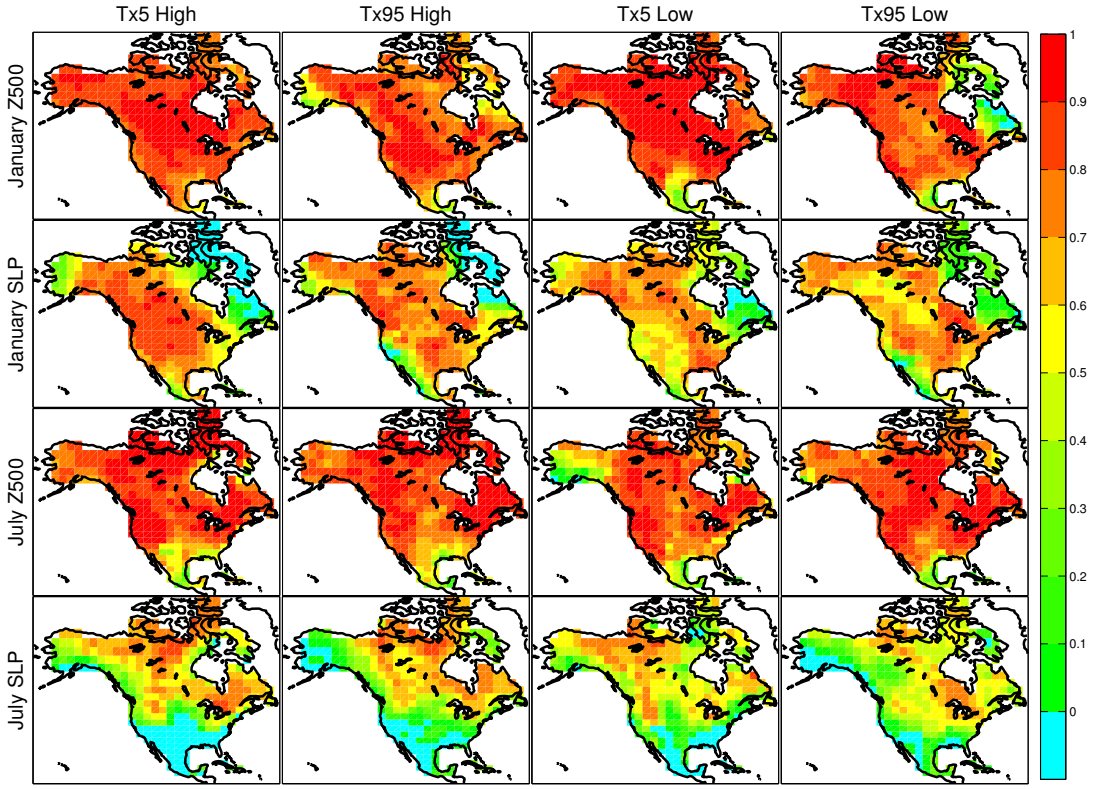

Figure 4.5. Same as figure 4.4 except for an individual model that generally agrees well with observations (left two columns) and one for which the agreement is poorer (right two columns).

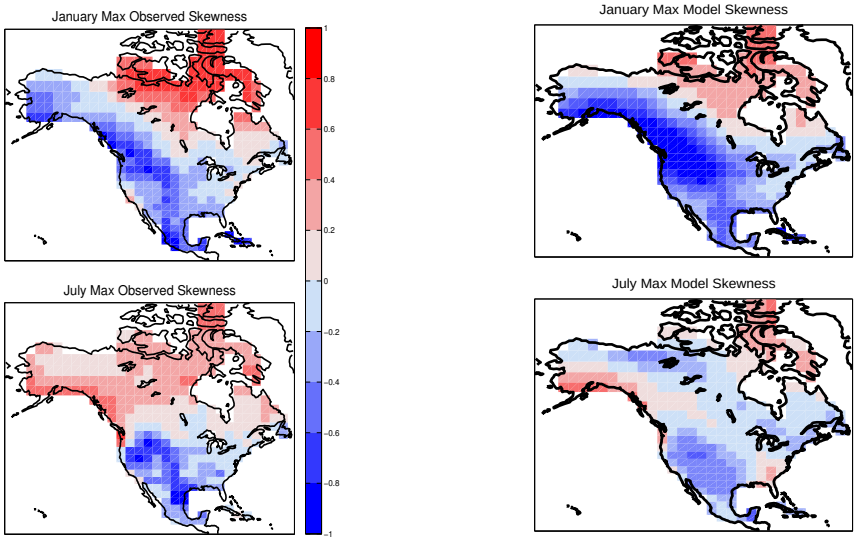

Figure 4.6. Skewness for the entire 30 years of temperature anomalies for January (top) and July (bottom) daily temperatures. The left two panels are observed skewness and the right two are the mean skewness value for the seventeen models.

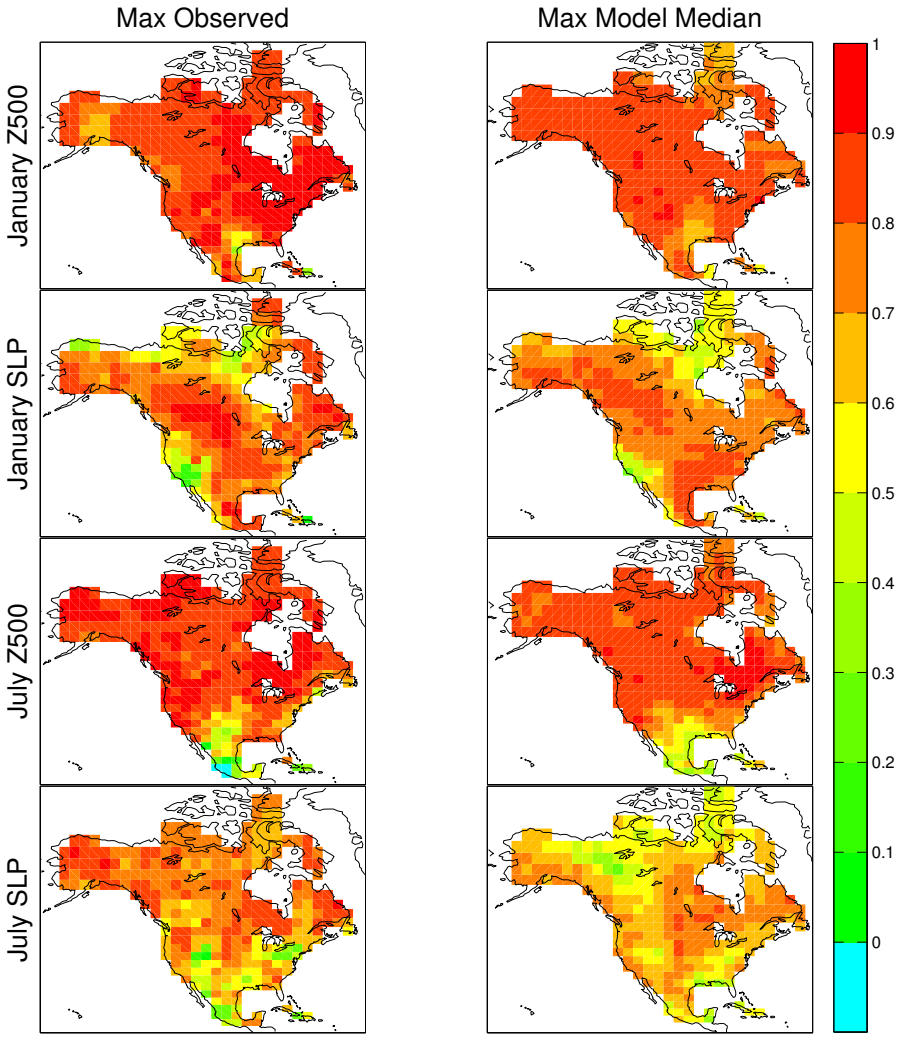

Figure 4.7. Maps of symmetry for observations (left column) and the median values of the seventeen models (right column). All results are for daily maximum temperature extremes. The top four panels are for January and the bottom four are for July. The 1st and 3rd rows are for Z500 and the 2nd and 4th rows are for SLP.

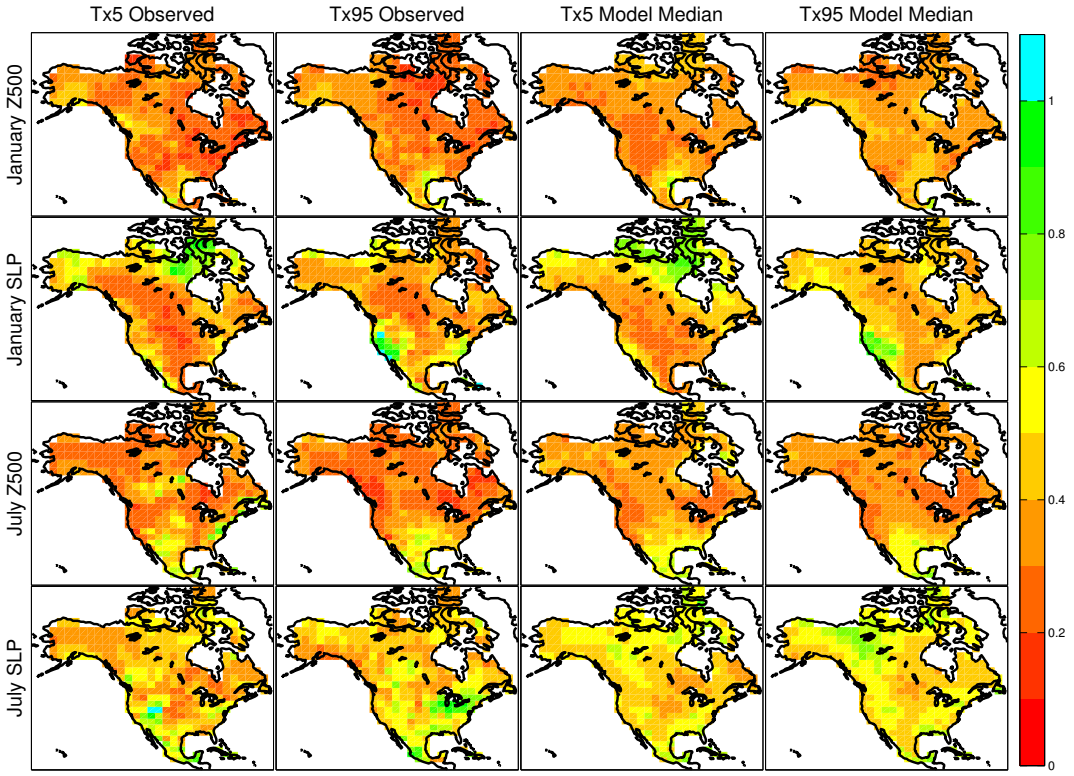

Figure 4.8. Maps of pattern linearity for observations (left two columns) and the median values of the seventeen modes (right two columns). The 1st and 3rd columns are for extreme cold maximum temperature patterns, and the 2nd and 4th columns are for extreme warm maximum temperature patterns. The top two rows are for January and the bottom two rows are for July. The 1st and third rows are for Z500 and the 2nd and 4th rows are for SLP.

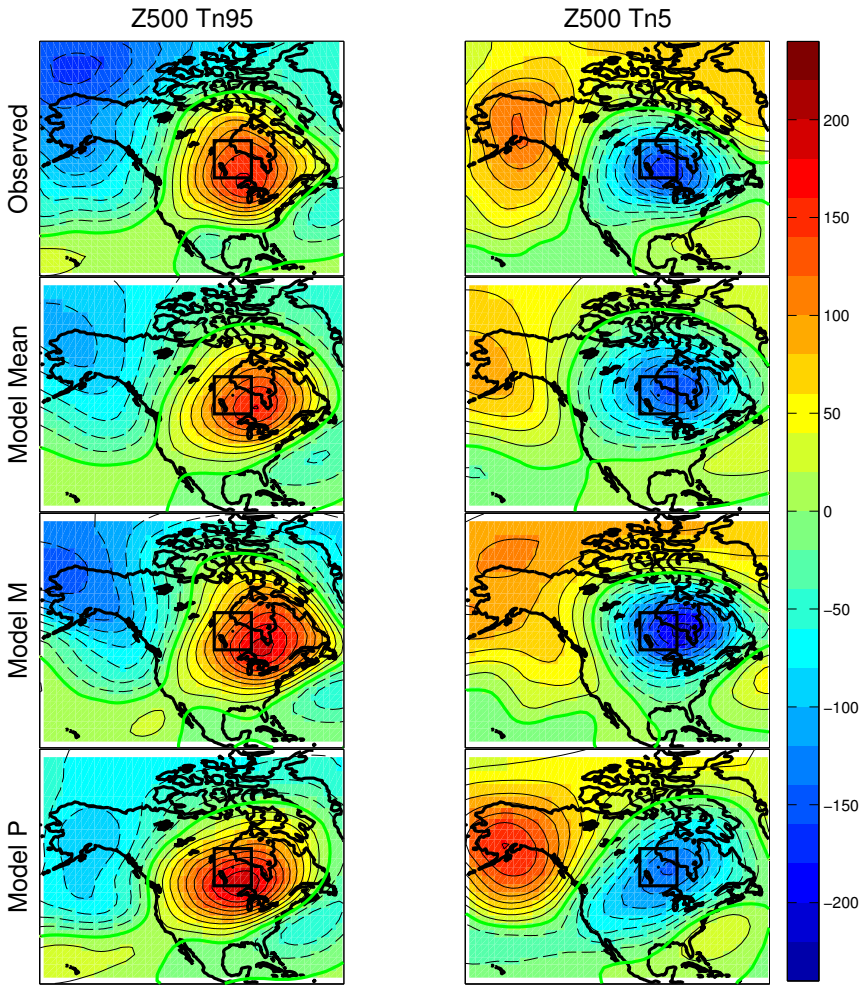

Figure 4.9. Maps of composite Z500 anomaly patterns for a grid cell at the center of the black box for extreme warm January minimum temperatures (left column) and extreme cold January minimum temperatures (right column) for Z500. From top to bottom, the rows represent the observed pattern, the multi-model mean pattern, the pattern simulated by Model M, and the pattern simulated by Model P. The zero contour line is highlighted in green. Units are m.

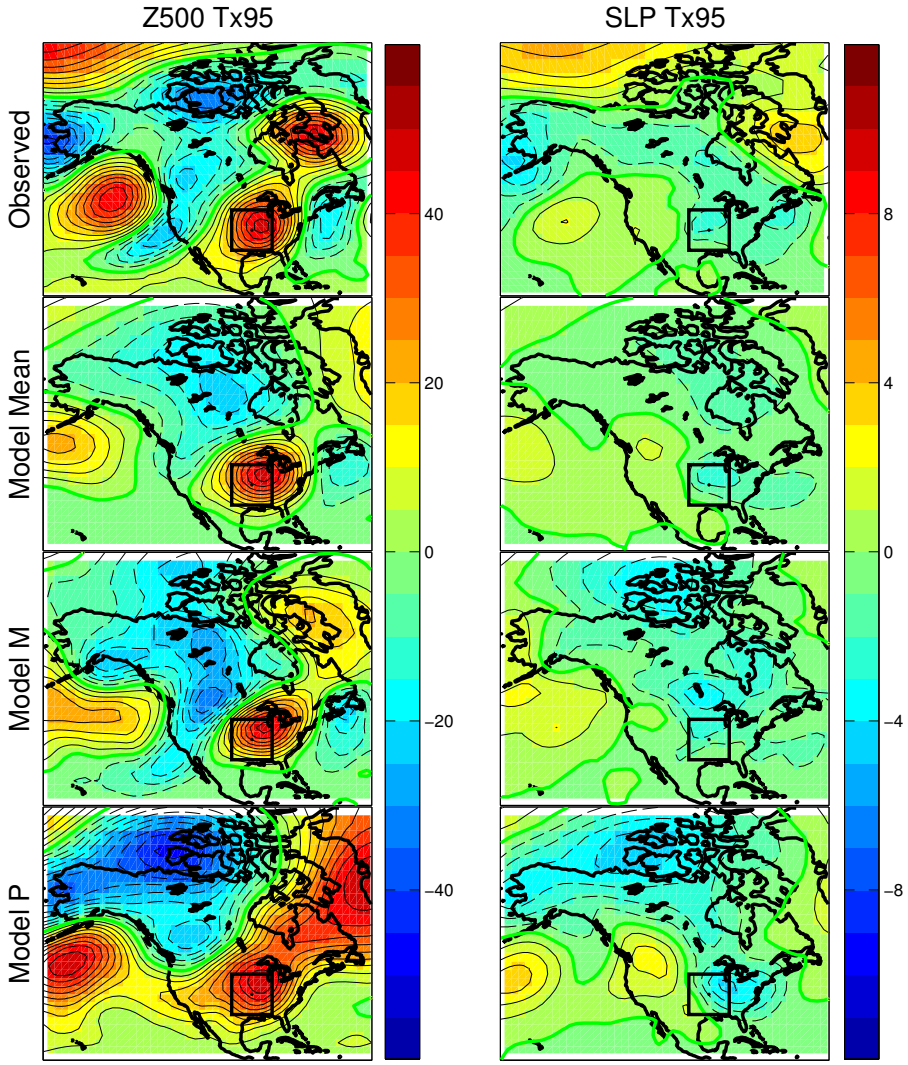

Figure 4.10. The same as Figure 4.9 except for Z500 (left column) and SLP (right column) anomaly patterns for July extreme warm maximum temperatures. Units are m (Z500) and hPa (SLP) anomalies.

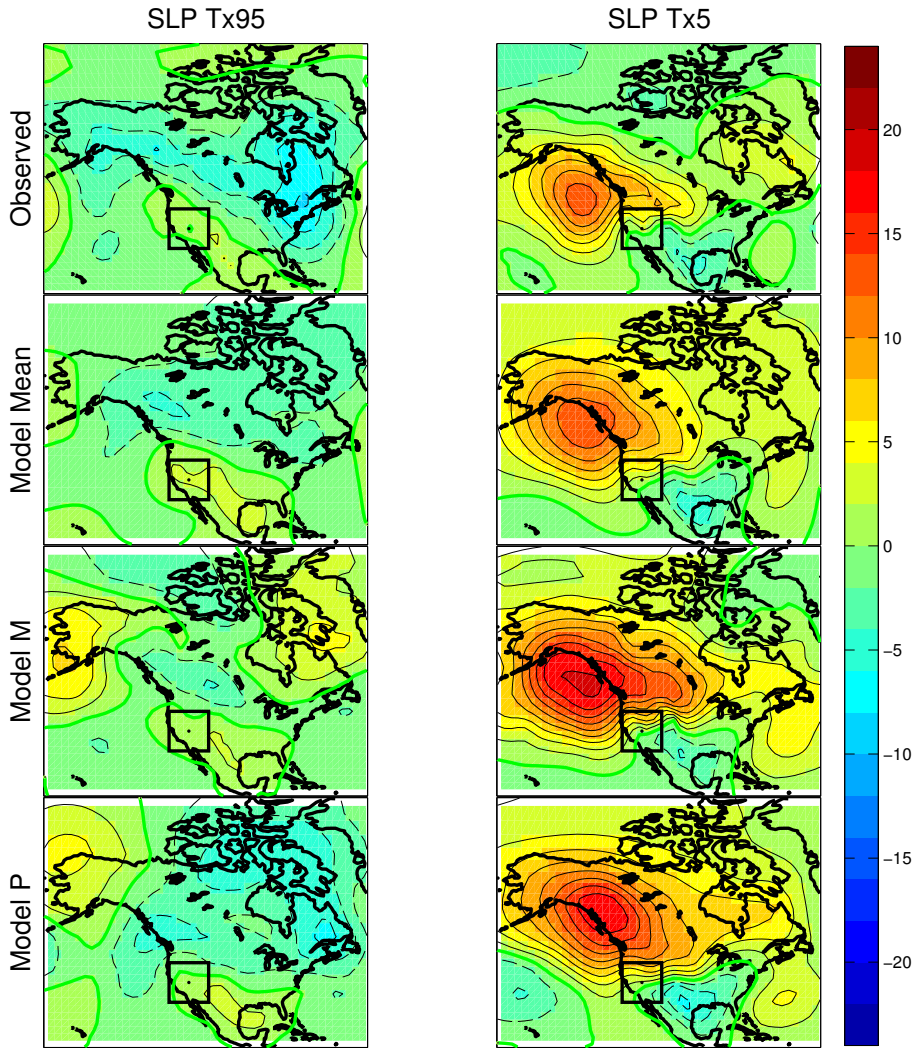

Figure 4.11. The same as Figure 4.9 except SLP patterns for extreme warm maximum temperatures (left column) and extreme cold maximum temperatures (right column). Units are hPa.

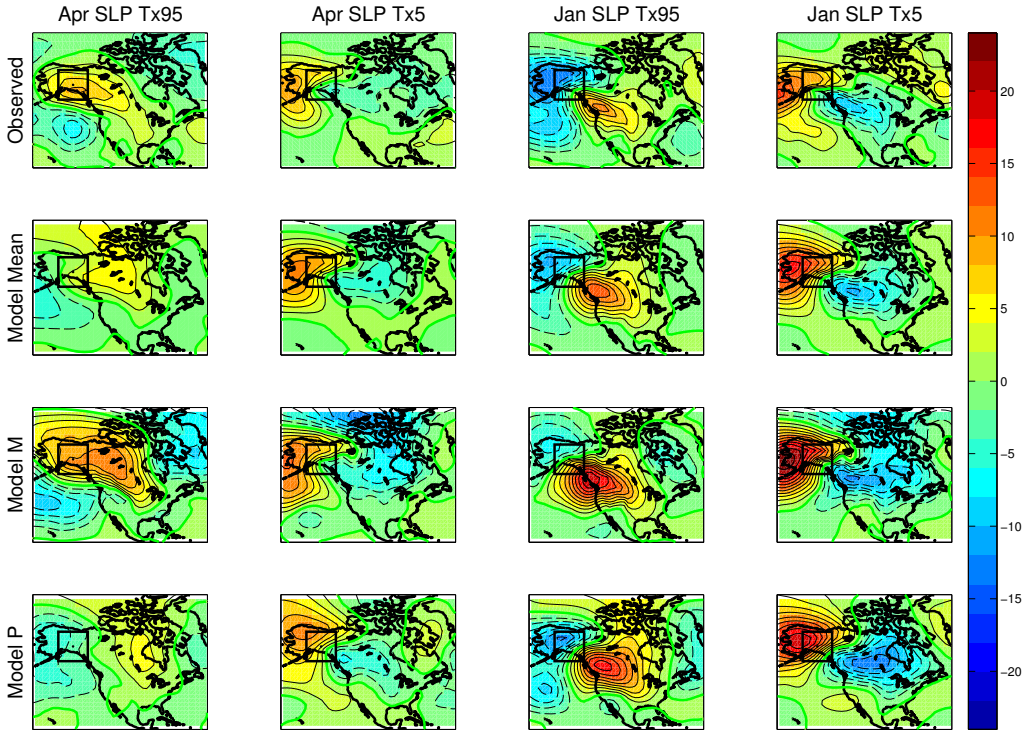

Figure 4.12. The same as Figure 4.9 except for patterns associated with extreme warm (first column) and cold (second column) maximum temperature days for April and extreme warm (third column) and cold (fourth column) maximum temperature days for January. Units are hPa.

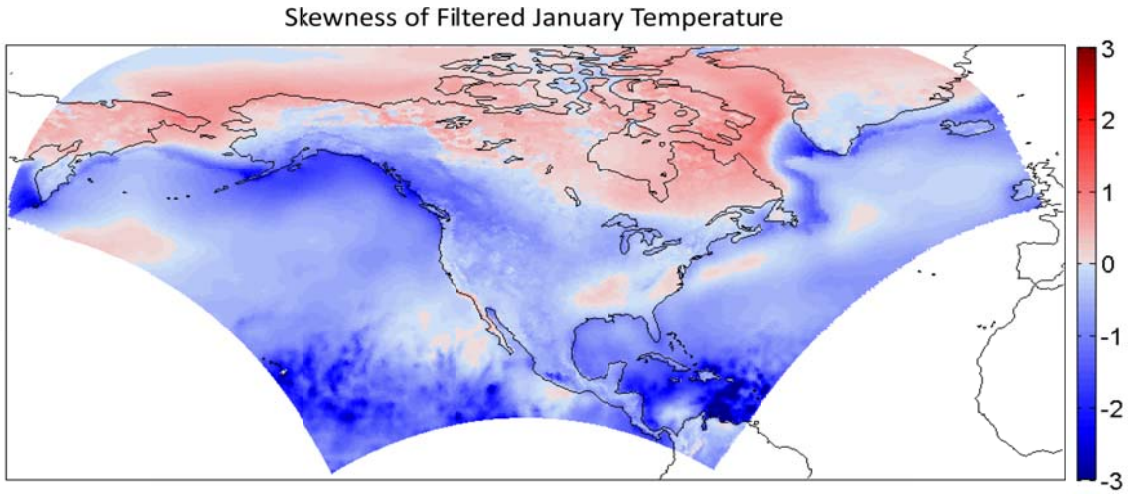

Figure 5.1. Skewness of temperature anomalies using North American Regional Reanalysis (NARR) data.

Appendix

A	GFDL-ESM2G
B	CMCC-CM
C	CanESM2
D	IPSL-CM5A-LR
E	INM-CM4
F	MPI-ESM-MR
G	BNU-ESM
H	GFDL-ESM2M
I	MPI-ESM-LR
J	FGOALS-g2
K	CNRM-CM5
L	IPSL-CM5A-MR
M	MRI-CGCM3
N	MIROC5
O	HadGEM2-CC
P	FGOALS-s2
Q	MIROC-ESM-CHEM

Table A.1. List of letters assigned to model names for Chapter 4.

References

Alexander, L. V., and Coauthors., 2006: Global observed changes in daily climate extremes of temperature and precipitation. *J. Geophys. Res*., **111**, D05109 doi:10.1029/2005JD006290.

Barnston, A. G., and R. E. Livezey, 1987: Classification, seasonality, and persistence of low-frequency atmospheric circulation patterns. *Mon. Wea. Rev.*, **115**, 1083-1126.

Beniston, M., 2004: The 2003 heat wave in Europe: A shape of things to come? An analysis based on Swiss climatological data and model simulations. *Geophys. Res. Lett.*, **31**, L02202, doi:10.1029/2003GL018857.

Brown, P. J., R. S. Bradley, and F. T. Keimig, 2010: Changes in extreme climate indices for the Northeastern United States, 1870-2005. *J. Climate*, **23**, 6555-6572.

Brown, S. J., J. Caesar, and C. A. T. Ferro, 2008: Global changes in extreme daily temperature since 1950. *J. Geophys. Res.*, **113**, D05115, doi:10.1029/2006JD008091.

Caesar, J., L. Alexander, and R. Vose (2006), Large-scale changes in observed daily maximum and minimum temperatures: Creation and analysis of a new gridded data set. *J. Geophys. Res.*, **111**, D05101, doi:10.1029/2005JD006280.

Cassano, E. N., J. J. Cassano, and M. Nolan, 2011: Synoptic weather pattern controls on temperature in Alaska, *J. Geophys. Res.*, **116**, D11108, doi:10.1029/2010JD15341.

Cattiaux, J., R. Vautard, C. Cassou, P. Yiou, V. Masson-Delmotte, and F. Codron, 2010: Winter 2010 in Europe: A cold extreme in a warming world. *Geophy. Res. Lett.*, **37**, doi:10.1029/2010GL044613.

Christidis, N., P. A. Stott, S. Brown, G. Hegerl, and J. Caesar, 2005: Detection of changes in temperature extremes during the second half of the 20th century. *Geophys. Res. Lett.*, **32**, doi:10.1029/2005GL023885.

Christidis, N., P. A. Stott, and S. Brown, 2011: The role of human activity in the recent warming of extremely warm daytime temperatures. *J. Climate*, **24**, 1922-1930.

Dole, R., M. Hoerling, J. Perlwitz, J. Eischeid, P. Pegion, T. Zhang, X.-W. Quan, T. Xu, and D. Murray, 2011: Was there a basis for anticipating the 2010 Russian heat wave? An analysis based on Swiss climatological data and model simulations. *Geophys. Res. Lett.*, **38**, L06702, doi:10.1029/2010GL046582.

Donat, M. G., and L. Alexander, 2012: The shifting probability distribution of global daytime and night-time temperatures. *Geophys. Res. Lett.*, **39**, L14707, doi:1029/2012GL052459.

Easterling, D. R., G. A. Meehl, C. Parmesan, S. A. Changnon, T. R. Karl, and L. O. Mearns, 2000: Climate extremes: Observations, modeling, and impacts. *Science*, **289**, 2068-2074.

Fischer, E. M., S. I. Seneviratne, P. L. Vidale, D. Lüthi, and C. Schär, 2007: Soil moisture-atmosphere interactions during the 2003 European summer heat wave. *J. Climate*, **20**, 5081-5099.

Frich, P., V. Alexander, P. Della-Marta, B. Gleason, M. Haylock, A. M. G. Klein Tank, T. Peterson, 2002: Observed coherent changes in climatic extremes during the second half of the twentieth century. *Climate Res.*, **19**, 193-212.

Gershunov, A., and T. P Barnett, 1998: ENSO influence on intraseasonal extreme rainfall and temperature frequencies in the contiguous United State: Observations and model results. *J. Climate*, **11**, 1575-1586.

Gleckler, P. J., K. E. Taylor, and C. Doutriaux, 2008: Performance metrics for climate models. *J. Geophys. Res.*, **113**, D06104, doi:10.1029/2007JD008972.

Griffiths, M. L., and R. S. Bradley, 2007: Variations of twentieth-century temperature and precipitation extreme indicators in the Northeast United States. *J. Climate*, **20**, 5401-5417.

Guirguis, K., A. Gershunov, R. Schwartz, and S. Bennett, 2011: Recent warm and cold daily winter temperature extremes in the Northern Hemisphere. *Geophys. Res. Lett.*, **38**, doi:10.1029/2011GL048762.

Hegerl, G. C., F. W. Zwiers, P. A. Stott, and V. V. Kharin, 2004: Detectability of anthropogenic changes in annual temperature and precipitation extremes. *J. Climate*, **17**, 3683-3700.

Higgins, R. W., A. Leetmaa, and V. E. Kousky, 2002: Relationships between climate variability and winter temperature extremes in the United States. *J. Climate*, **15**, 1555-1572.

Horel, J. D., and J. M. Wallace, 1981: Planetary-scale atmospheric phenomena associated with the Southern Oscillation. *Mon. Wea. Rev.*, **109**, 813-829.

Hurrell, J. W., Y. Kushnir, G. Ottersen, and Martin Visbeck, 2003: An overview of the North Atlantic Oscillation. *The North Atlantic Oscillation: Climate Significance an Environmental Impact*, *Geophys. Monogr*., Vol. 134, Amer. Geophys. Union, 1-35.

Kalnay, E., and Coauthors., 1996: The NCEP/NCAR 40-year reanalysis project. *BAMS*, **77**, 437-471.

Kenyon, J., and G. C. Hegerl, 2008: Influence of modes of climate variability on global temperature extremes. *J. Climate*, **21**, 3872-3889.

Kharin, V. V., and F. W. Zwiers, 2000: Changes in the extremes in an ensemble of transient climate simulations with a coupled atmosphere-ocean GCM. *J. Climate*, **13**, 3760-3788.

Kharin, V. V., and F. W. Zwiers, 2005: Estimating extremes in transient climate change simulations. *J. Climate*, **18**, 1156-1173.

Kharin, V. V., F. W. Zwiers, X. Zhange, and G. C. Hegerl, 2007: Changes in temperature and precipitation extremes in the IPCC ensemble of global coupled model simuations. *J. Climate*, **20**, 1419-1444.

Kiladis, G. N., and H. F. Diaz, 1989: Global climatic anomalies associated with extremes in the southern oscillation. *J. Climate*, **2**, 1069-1090.

Kodra, E., K. Steinhaeuser, and A. R. Ganguly, 2011: Persisting cold extremes under 21st-century warming scenarios. *Geophys. Res. Lett.*, **38**, L08705, doi:10.1029/2011GL047103.

Lau, Ngar-Cheung, Mary Jo Nath, 2012: A Model Study of Heat Waves over North America: Meteorological Aspects and Projections for the Twenty-First Century. *J. Climate*, **25**, 4761–4784.

Liang, X., D. P. Lettenmaier, E. F. Wood, and S. J. Burges, 1994: A Simple hydrologically Based Model of Land Surface Water and Energy Fluxes for GSMs, *J. Geophys. Res.*, **99**, 14,415-14,428.

Loikith, P. C., and A. J. Broccoli, 2012: Characteristics of observed atmospheric circulation patterns associated with temperature extremes over North America. *J. Climate*, In Press.

Lu, J., G. A. Vecchi, and T. Reichler, 2007: Expansion of the Hadley cell under global warming. *Geophys. Res. Lett., **34**, L06805, doi:10.1029/2006GL028443.*

Meehl, G. A., and C. Tebaldi, 2004: More intense, more frequent, and longer lasting heat waves in the 21st century. *Science*, **305**, 994-997.

Meehl, G.A., T.F. Stocker, W.D. Collins, P. Friedlingstein, A.T. Gaye, J.M. Gregory, A. Kitoh, R. Knutti, J.M. Murphy, A. Noda, S.C.B. Raper, I.G. Watterson, A.J. Weaver and Z.-C. Zhao, 2007: Global Climate Projections. In: Climate Change 2007: The Physical Science Basis. Contribution of Working Group I to the Fourth Assessment Report of the Intergovernmental Panel on Climate Change [Solomon, S.,D. Qin, M. Manning, Z. Chen, M. Marquis, K.B. Averyt, M. Tignor and H.L. Miller (eds.)]. Cambridge University Press, Cambridge, United Kingdom and New York, NY, USA.

Meehl, G. A., C. Tebaldi, G. Walton, D. Easterling, and L. McDaniel, 2009: Relative increase of record high maximum temperatures compared to record low minimum temperatures in the U.S. *Geophys. Res. Lett.*, **36**, L23701, doi:10.1029/2009GL040736.

Morak, S., G. C. Hegerl, and J. Kenyon, 2011: Detectable regional changes in the number of warm nights. *Geophys. Res. Lett.*, **38**, L17703, doi:10.1029/2011GL048531.

Otto, F. E. L., N. Massey, G. J. van Oldenborgh, R. G. Jones, and M. R. Allen, 2012: Reconciling two approaches to attribution of the 2010 Russian heat wave. *Geophy. Res. Lett.*, **39**, L04702, doi:10.1029/2011GL050422.

Quadrelli, R., and J. M. Wallace, 2004: A simplified linear framework for interpreting patterns of Northern Hemisphere wintertime climate variability. *J. Climate*, **17**, 3728-3744.

Rahmstorf, S. and D. Coumou, 2011: Increase of extreme events in a warming world. *Proc. Nat. Acad. Sci.*, doi:10.1073/pnas.1101766108.Ruff, T. W., and J. D. Neelin, 2012: Long tails in regional surface temperature probability distributions with implications for extremes under global warming. *Geophys. Res. Lett.*, doi:10.1029/2011GL050610.

Ropelewski, C. F., and M. S. Halpert, 1987: Global and regional scale precipitation patterns associated with the El Nino/Southern Oscillation. *Mon. Wea. Rev.*, **115**, 1606-1626.

Rowe, C. M., and L. E. Derry, 2012: Trends in record-breaking temperatures for the conterminous United States. *Geophys. Res. Lett.*, **39**, L16703, doi:1029/2012GL052775.

Ruff, T. W., and J. D. Neelin, 2012: Long tails in regional surface temperature probability distributions with implications for extremes under global warming. *Geophys. Res. Lett.*, **39**, doi:10.1029/2011GL050610.

Schär, C., P. L. Vidale, D. Lüthi, C. Frei, C. Häberli, M. A. Liniger, and C. Appenzeller, 2004: The role of increasing temperature variability in European summer heatwaves. *Nature*, **427**, 332-336.

Seidel, D. J., Q. Fu, W. J. Randel, T. J. Reichler, 2008: Widening of the tropical belt in a changing climate. *Nature Geoscience*, **1**, 21-24.

Stott, P. A., D. A. Stone, and M. R. Allen, 2004: Human contribution for the European heatwave of 2003. *Nature*, **432**, 610-614.

Taylor, K. E., R. J. Stouffer, and G. A.Meehl: An overview of CMIP5 and the experiment design. *Bull. Amer. Meteor. Soc.*, **93**, 485-498.

Tebaldi, C., K. Hayhoe., J. M. Arblaster, and G. A. Meehl, 2006: Going to the extremes, an intercomparison of model-simulated historical and future changes in extreme events. *Climatic Change*, **79**, 185-211.

Thompson, D. W. J., and J. M. Wallace, 1998: The Arctic Oscillation signature in the wintertime geopotential height and temperature fields. *Geophys. Res. Lett.*, **9**, 1297-1300.

Thompson, D. W. J., and J. Wallace, 2000: Annular modes in the extratropical circulation. Part I: Month-to-month variability. *J. Climate*, **13**, 1000-1016.

Thompson, D. W. J., and J. M. Wallace, 2001: Regional climate impacts of the Northern Hemisphere annular mode. *Science*, **293**, 85-89.

Trenberth, K. E., 1997: The Definition of El Niño. *Bull. Amer. Meteor. Soc.*, **78**, 2771-2777.

Vavrus, S., J. E. Walsh, W. L. Chapman, and D. Portis, 2006: The behavior of extreme cold air outbreaks under greenhouse warming. *Int. J. Climatology*, **26**, 1133-1147.

Wallace, J. M., and D. S. Gutzler, 1981: Teleconnections in the geopotential height field during the Northern Hemisphere winter. *Mon. Wea. Rev.*, **109**, 784-812.

Wang, C, H. Liu, and S.-K. Lee, 2010: The record-breaking cold temperatures during the winter of 2009/2010 in the Northern Hemisphere. *Atmos. Sci. Let.*, **11**, 161-168.

Weisheimer, A., F. J. Doblas_Reyes, T. Jung, and T. N. Palmer, 2011: On the predictability of the extreme summer 2003 over Europe. *Geophys. Res. Lett.*, **38**, L05704, doi:10.1029/2010GL046455.

Wettstein, J. J., and L. O. Mearns, 2002: The Influence of the North Atlantic- Arctic Oscillation on mean, variance, and extremes of temperature in the Northeastern United States and Canada. *J. Climate*, **15**, 3586-3600.

Yu, J.-Y., Y. Zou, S. T. Kim, and T. Lee, 2012: The changing impact of El Niño on US winter temperatures. *Geophys. Res. Lett.*, **39**, L15702,doi:10.1029/2012GL052483.

Yin, J. H., 2005: A consistent poleward shift in the storm tracks in simulations of 21st century climate. *Geophys. Res. Lett.*, **32**, L18701, doi:10.1029/2005GL023684.

Zwiers, F. W., X. Zhang, and Y. Feng, 2011: Anthropogenic influence on long return period daily temperature extremes at regional scales. *J. Climate*, **24**, 881-892.

Acknowledgement of Previous and Future Publication

Much of this work is comprised of journal articles that are either accepted for publication or in preparation for review. Chapter 2 is comprised almost entirely of the following paper that is currently in press for the American Meteorological Society's *Journal of Climate*:

Loikith, P. C., and A. J. Broccoli, 2012: Characteristics of Observed Atmospheric Circulation Patterns Associated with Temperature Extremes over North America, *J. Climate*, in press.

Chapter 3 and 4 are comprised almost entirely of the following papers that are in preparation for submission to the *Journal of Climate*:

Loikith, P.C., and A. J. Broccoli: The Influence of Recurrent Modes of Climate Variability on the Occurrence of Extreme Temperatures over North America, *J. Climate*, in prep.

Loikith, P.C., and A.J. Broccoli: Comparison between Observed and Model Simulated Atmospheric Circulation Patterns Associated with Extreme Temperature Days over North America using CMIP5 Historical Simulations, *J. Climate*, in prep.